CHALMERS
UNIVERSITY OF TECHNOLOGY

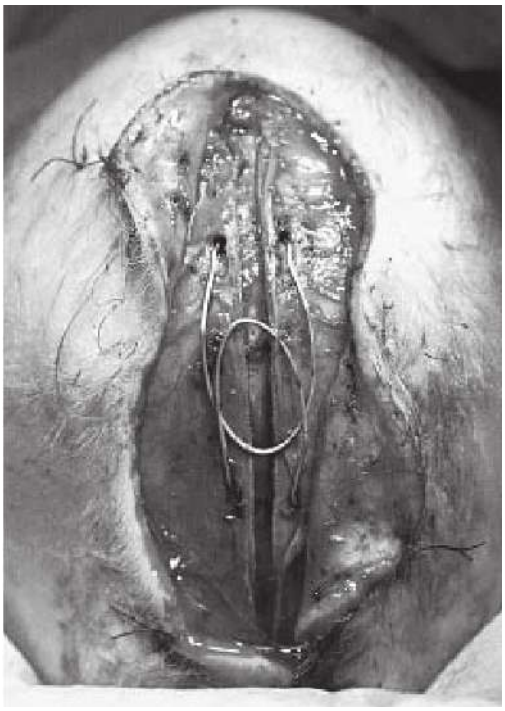

Development of Resorbable “Springs” for Surgery

Material Properties and Biocompatibility

Master Degree project report in Biomedical Engineering

SARA BAUER

DEPARTMENT OF APPLIED CHEMISTRY & DEPARTMENT OF CHEMICAL BIOLOGY, LIFE SCIENCES

CHALMERS UNIVERSITY OF TECHNOLOGY
Gothenburg, Sweden 2024
www.chalmers.se

Degree project report 2024

Development of Resorbable "Springs" for Surgery

Material Properties and Bicompatibility

SARA BAUER

CHALMERS
UNIVERSITY OF TECHNOLOGY

Department of Chemistry and Chemical Engineering & Department of Chemical Biology, Life sciences
Chalmers University of Technology
Gothenburg, Sweden 2024

Development of Resorbable “Springs” for Surgery
Material Properties and Bicompatibility
SARA BAUER

Supervisor: Alexandra Stubelius, Chemical Biology
Examiner: Anna Ström, Applied Chemistry

Master Degree project report 2024
Department of Chemistry and Chemical Engineering & Department of Chemical Biology, Life sciences
Chalmers University of Technology
SE-412 96 Gothenburg
Sweden
Telephone +46 31 772 1000

Cover: Spring assisted surgery for sagittal craniosynostosis, with permission from ref.[73].

Typeset in LaTeX
Gothenburg, Sweden 2024

Development of Resorbable “Springs” for Surgery
Material Properties and Biocompatibility
SARA BAUER
Department of Chemistry and Chemical Engineering & Department of Chemical Biology, Life sciences
Chalmers University of Technology

Abstract

The demand for replicating the functionality of conventional stainless steel springs with degradable and biocompatible materials has led to the exploration of alternative methods. Current trends focus on understanding the genetic and cellular causes of craniosynostosis rather than its treatment. Nonetheless, research has investigated gelatin scaffolds supporting suture regeneration with mesenchymal stem cells, protein-releasing Titania nanotubular implants that inhibit bone formation, and a bioabsorbable material blend of poly(lactic-co-glycolic acid) (PLGA) and polyisoprene (PI). Furthermore, advancements in 3D printing technology now enable the production of implantable objects, sparking interest in printing cranial spring implants, particularly for addressing sagittal craniosynostosis.
Polylactic acid (PLA) was 3D printed, mechanical strength tested using force strain measurements and degradation was followed using PBS. PLGA/PI blends were prepared according to the suggested method, miscibilty and degradation in PBS at pH 7.4 and 5 were tested.
Printed PLA samples with different filling patterns demonstrated high load-bearing capacity, averaging 2109 N, which scales to 527 N for implant size, surpassing the 8 N threshold of stainless steel springs. After one month, PLA showed no significant degradation, suggesting that this material lasts longer than the expected 4-6 months.
A literature review was also conducted to assess existing methods and future directions in the field. This review provided valuable context for understanding current practices and emerging trends.
Research into alternative materials led to the discovery of a promising PLGA/PI blend that had already been tested in rabbits [9]. The molding process and the immiscibility of the material became a major limitation for its use as a potential implant, even tough its degradation process seems promising.

Keywords: sagittal craniosynostosis, calvarial reconstruction, 3D printing, cellprene, PLGA degradation

Acknowledgements

I would like to express my gratitude to my supervisor, Alexandra Stubelius, and my examiner, Anna Ström, for their support and guidance throughout this project.

I am also grateful to all the wonderful colleagues in the office. Thank you for welcoming me so warmly, showing me around the labs, and assisting me with the numerous "little" problems that arose.

Lastly, a huge thanks goes to my family. Your constant encouragement, love, and support have been the foundation upon which I could build and complete this project. I am profoundly grateful for everything you have done to make this possible. Danke. De gra.

Sara Bauer, Gothenburg, June 2024

List of Acronyms

Below is the list of acronyms that have been used throughout this thesis listed in alphabetical order:

Ca^{2+}	Calcium
CO_2	Carbon Dioxide
CSF	Cerebrospinal Fluid
CT	Computed Tomography
DL-PLGA	Poly(DL-lactic-co-glycolic acid)
ESC	Endoscopic Strip Craniectomy
ESC-H	Endoscopic Strip Craniectomy with use of postoperative molding helmet
FGFR1-3	Fibroblast Growth Factor Receptors 1-3
GOSH	Great Ormond Street Hospital
GPC3	Glypican 3
Gli1+	GLI Family Zinc Finger 1 Positive
HCO_3^-	Bicarbonate
Mg^{2+}	Magnesium
MSC	Mesenchymal Stem Cells
Mn	Number average molecular weight
Mw	Molecular Weights
NFPA	National Fire Protection Association
PBS	Phosphate-buffered Saline
PCL	Polycaprolactone
PDLLA	Poly(D,L-lactic acid)
PI	Polyimide
PLA	Polylactic Acid
PLGA	Poly(lactic-co-glycolic acid)
SAC	Spring Assisted Cranioplasty
SBF	Simulated Body Fluid
Tg	Glass Transition Temperature
THF	Tetrahydrofuran
TNT/Ti	Titania Nanotubular Implants loaded with Glypican 3
TWIST1	Twist-related protein 1
-COOH	Carboxyl

Contents

List of Figures

List of Tables

1

Introduction

Each year approximately 1 in 2,100-2,500 infants developes craniosynostosis [1], a condition that involves the premature fusion of cranial sutures and can lead to severe damage of the brain development and various severe medical complications, including brain damage, developmental delays, and visual and breathing issues [1, 2, 3].

The skull grows extremely fast in utero and in the first years of life. The brain volume is already at 40% of a adult brain volume as soon as the baby is born and it increases to 80% when the child reaches 3 years. At 7 years it is about 90%. Mature suture closure occurs by 12 years of age, but completion continues into the third decade of life and beyond [5].

The term *craniosynostosis* was first introduced by Virchow in 1851, and until today his findings are known as the Virchow's law: The premature fusion of the sutures does not allow an active brain growth and passive growth/adaption of the skull in parallel direction to the closed suture. Instead it will compensate the growth in the direction of lowest resistance, perpendicular to the affected suture. The modern era of craniofacial surgery started in the 1960s with Tessier as the first who established craniofacial teams in Paris [11, 16, 28].

Dealing with skull deformities in infants remains a complex task for diagnosis and treatment, since the growth of the infants brain is limited by the deformities. It is crucial to differentiate between common deformational plagiocephaly, which results from prolonged back sleeping of the infants in the same position, and the more severe craniosynostosis, which can occur independently or as part of a syndrome. In deformational plagiocephaly, there is no fusion of the skull bones; however, flat spots on the head develop on the side or back. In contrast, craniosynostosis involves the fusion of skull bones, resulting in a similar head shape as the deformational plagiocephaly [3, 6].

Various types and degrees of skull deformities exist, where some cases necessitate surgical intervention. Among these, sagittal craniosynostosis stands out as the most frequently encountered [6].

1.1 Aim

My aim was to address the identified requirement of minimizing the amount of SAC surgeries by eliminating the necessity for a second surgery to remove the springs. This will be achieved by introducing "resorbable springs" as a practical substitute for traditional stainless steel springs.
Furthermore, a review of alternative methods currently in use will be conducted to evaluate alternative stainless steel springs and multiple surgeries.

The primary focus of the work was the material strength properties, of selected medically approved and biodegradable materials, such as Polylactic Acid and Poly(lactic-co-glycolic acid). Moreover an investigation into the impact of various 3D printing shapes and infills on the overall material strength was conducted.
Additionally, the study compared and analyzed the degradation effects of the different 3D prints, aiming to remove the second surgery for removal of the material.

More specific aims were to define:

- To what extent does the 3D print pattern impact the strength of PLA and PLA/PLGA blends in relation to its volume, taking into account the desired strength of surgical spring being 8N?
- What impact does pore size or 3D print pattern have on material degradation and strength, and how does the water degradation rate differ between PLA and PLA/PLGA blends?

1.2 Limitations / Demarcations

The scope of the master's thesis project is restricted to the examination of non syndromic sagittal craniosynostosis in infants. The selection of materials is limited to those acknowledged for degradation via hydrolysis. Materials that are not biocompatible or that initiate osteogenesis will not be studied. Additionally, a 3D printer without a dual-nozzle and without angle rotation will be used, given the limitations of the available printers in the department. Furthermore, the limited time available imposed restrictions on experimenting with different blends.
The project does not factor in the expansion and contraction of the material.

2
Theory

In this chapter, the theory relevant for the different parts of the project is described and explained.

2.1 Craniosynostosis

The sutures in an infant's skull serve the purpose of facilitating passage through the birth canal and allowing for brain growth. However, in some cases, these sutures may close earlier than expected, resulting in a condition known as craniosynostosis. Craniosynostosis is characterized by cranial deformation and can lead to problems all over the body [29].
Craniosynostosis can be categorized as either simple or complex, depending on the number of sutures involved. When a single suture is affected, it is termed simple craniosynostosis, whereas involvement of multiple sutures indicates complex craniosynostosis [14, 15].
Additionally, craniosynostosis can be further classified as syndromic or non-syndromic. Syndromic craniosynostosis is associated with conditions such as Apert, Crouzon, or Pfeiffer syndrome, while non-syndromic craniosynostosis occurs as an isolated disorder and is more common [15].
Various factors, including environmental influences (such as intrauterine fetal head constraint, abnormal positioning, and prenatal exposure to teratogens) and genetic predispositions (such as single gene mutations and chromosome abnormalities), contribute to the development of craniosynostosis [15].
Diagnosis of craniosynostosis typically occurs within the first year of life. Clinical assessment involves determining the presence of craniosynostosis, identifying any associated syndromes, and deciding on the need for urgent or elective management [15].
It's essential to distinguish craniosynostosis from positional plagiocephaly, a more common cranial deformity. Unlike craniosynostosis, positional plagiocephaly does not involve premature fusion of sutures and is managed through positional changes and the so called "tummy time". The flattening will diminish with the natural growth of the child. Clinical examination and, if necessary, radiographic imaging (x-ray and CT) help differentiate between the two conditions [15, 16].

2.1.1 Sagittal craniosynostosis

Sagittal craniosynostosis, also known as scaphocephaly (derived from the Greek word "skaphos" meaning boat-head), is the most prevalent form of craniosynostosis [4, 10]. It is characterized by narrowing at the biparietal region and bilateral bulging of the frontal and occipital regions or both [11]. Another term for sagittal craniosynostosis is 'dolichocephaly', with the prefix 'dolicho-' denoting elongation in Greek. This appearance arises from premature suture closure, causing the brain to grow in a perpendicular direction [11]. Sagittal craniosynostosis accounts for 40-60% of all craniosynostosis cases [5, 14], with a male-to-female ratio of 3:1 [12, 13, 14].

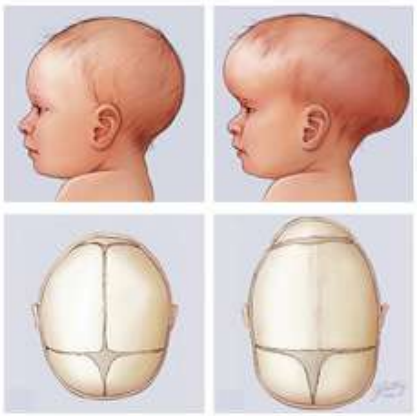

Figure 2.1: Sagittal craniosynostosis [4]

2.2 Sutures and fontanelles of the head

In this section a picture is shown in order to get an overview of the medical terminology regarding the head.

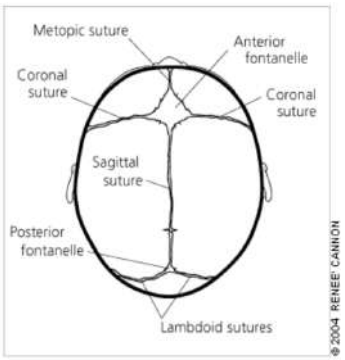

Figure 2.2: Sutures on the head, seen from above, with permission from ref. [5]

2.3 Treatments

The treatment approach for craniosynostosis varies widely, with decisions influenced by factors such as the infant's age and the severity of the condition. Initially, clinicians must determine whether surgical intervention is necessary or if alternative methods suffice. Age and presentation play crucial roles in this decision-making process. Treatment options span a spectrum, ranging from conservative measures like helmet therapy for mild cases to surgical interventions for more severe presentations. Surgical approaches range from minimally invasive procedures to extensive

open craniotomies and reconstructions, depending on the severity of the case [15]. Due to the potential risks associated with untreated craniosynostosis, surgeons often opt for surgical intervention promptly following diagnosis [10].
Current surgical techniques can generally be categorized into three main types [10]:

- Calvarial Reconstruction Techniques
- Strip craniotomy
- Spring assisted cranioplasty

Each approach is tailored to the individual patient's needs and the specific characteristics of their condition.
Unfortunately, there is limited evidence regarding the optimal timing for surgical intervention in craniosynostosis cases. However, two primary approaches are commonly debated. The first suggests early surgery within the first month of life, while the second proposes surgery toward the end of the first year of life [17].
Opting for early surgery allows for a shorter duration of constriction, enabling normal brain development to commence sooner. However, this approach carries a higher risk of re-stenosis. Conversely, delaying surgery until later in the first year allows the infant's head to reach near-full size, potentially reducing the risk of re-stenosis during surgery, though it prolongs the period of constriction [17].

2.3.1 Minimal invasive techniques

These techniques are commonly employed in younger children due to their associated benefits, including reduced blood loss and shorter surgical duration. Typically, such surgeries are conducted in children under six months of age [23].

2.3.1.1 Strip craniectomy with use of postoperative molding helmet (ESC-H)

ESC-H is a minimally invasive technique that has gained popularity due to its reduced blood loss and faster surgery times.
In ESC-H for sagittal craniosynostosis, two transverse cuts are made behind the anterior fontanelle and in front of the lambdoid suture. The periosteum and dura are dissected along the suture, and an endoscope is inserted to provide illumination for monitoring the dissection progress. Bone is cut using heavy scissors, with the incision typically measuring 2-4 cm. The affected bone is then removed, bleeding is controlled, and the area is sutured closed, see Fig.2.3 [18, 20, 21].
Once initial swelling subsides and stitches are removed (typically within one week), a custom cranial molding helmet is designed for the child to promote balanced head growth. The individual modifications of the helmet are crucial for the success of this procedure [18].

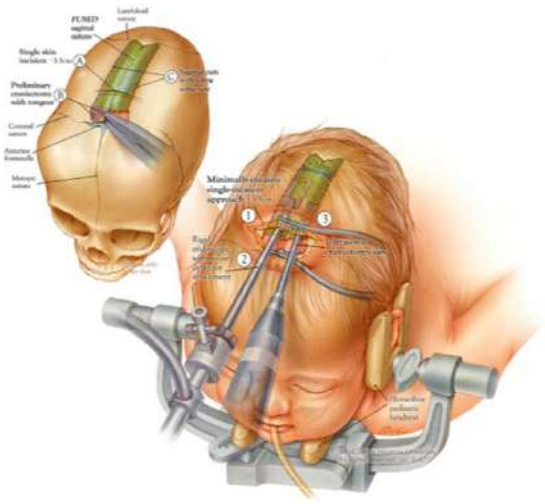

Figure 2.3: ESC, with permission from ref. [21]

Unlike spring or distraction techniques, which primarily influence skull growth in one dimension, the helmet allows growth in all three dimensions, with adjustments made accordingly over time. Helmets are typically worn until 12 to 18 months of age [18, 20].

2.3.1.2 Spring assisted cranioplasty (SAC)

SAC, introduced in 1998 by Lauritzen et al., emerged as an alternative to traditional open vault surgeries for treating craniosynostosis [10]. Regarded as one of the newer techniques in the field, SAC offers a promising approach to addressing craniosynostosis [19].
The treatment process for sagittal synostosis with SAC begins with a scalp incision while the infant is positioned prone. A rectangular craniotomy is then performed, followed by two parasagittal osteotomies extending from the coronal to lambdoid sutures. Typically, the osteotomies fan out slightly posteriorly as they reach the lambdoid sutures. Next, standardized metal springs are placed on each side of the osteotomy site, see Fig.2.4. These springs gradually expand, facilitating skull widening, see Fig. 2.5. Approximately 4-5 months after insertion, the springs are removed during a second surgery [22].

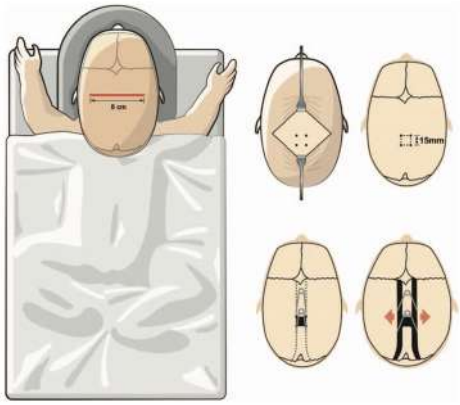

Figure 2.4: Schematic SAC procedure, with permission from ref.[23]

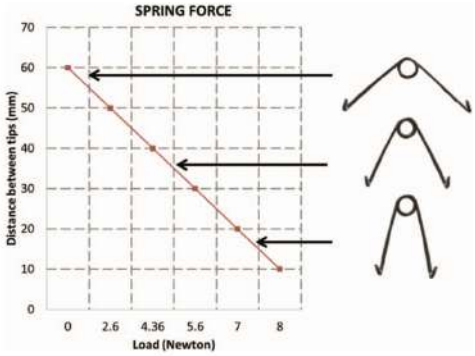

Figure 2.5: Spring opening and force over time, with permission from ref.[23]

At Sahlgrenska University Hospital in Gothenburg, Sweden, a new surgical approach is being employed where, instead of performing two parasagittal osteotomies around a closed suture, a craniectomy is conducted directly on the suture itself. Traditionally, two parasagittal osteotomies are performed to avoid damaging the midline bridging veins beneath the sagittal suture. However, a surgeon at Sahlgrenska emphasized that performing the craniectomy directly on the suture (midline craniotomy) leads to less blood loss and superior outcomes.
During the procedure, the springs are positioned 5 mm lateral to the osteotomy site, with small holes drilled to facilitate their placement [23, 24].
SAC has been a successful method for treating craniosynostosis for more than 20 years [7]. "It is a highly effective technique, however, removing the need of a second surgery reduce costs and risks associated to surgery of infants" (Professor Lars

Kölby, Department of Plastic Surgery at Sahlgrenska, personal communication, January 15, 2024).

2.4 Acting mechanical forces

Mechanical forces can be found throughout the body as a consequence of the physiological functioning of organs. Therefore it is essential to account these mechanical factors when it comes to the design of biomaterials [44].

2.4.1 Forces on sagittal craniosynostosis

Julius Wolff's seminal research in 1892 marked the beginning of studying the influence of biomechanical forces on bone adaptation [41]. Postnatally, the intricate development of the skull involves close physical and biochemical interactions between its bones, the brain, and the dura mater. Notably, research elucidates the vital role of signals from the dura mater in maintaining suture patency by influencing osteogenic cell populations [42].
The encapsulation of the brain within the dura, cranial vault, and calvarium forms a complex structure capable of withstanding and responding to biomechanical forces [31]. Integration at specific sites facilitates the generation of forces as the brain grows, exerting pressure against this encapsulating capsule. A change in the growth trajectory of one component can lead to corresponding changes in others, demonstrating the interconnected nature of cranial development [42].
Sagittal craniosynostosis exemplifies the dependence of brain growth on cranial sutures, a phenomenon discussed in various studies [42, 32]. Premature fusion of these sutures prompts compensatory growth in alternative directions to accommodate the expanding brain, as illustrated in Figure 2.6. Mechanical factors, including the brain itself, cerebrospinal fluid (CSF) dynamics, blood circulation, and the presence of thickened bone, collectively contribute to cranial enlargement, as depicted in Fig. 2.7. Premature suture fusion alters tensile strain patterns, potentially regulating both calvarial development and the fusion process itself [26, 32].
The increased stiffness of sutures in craniosynostosis likely results in a gradual reduction of tensile strain over time. Premature suture fusion appears to be associated with diminished intracranial pressures and decreased tensile strain at the sutures. Thus, it seems that tensile forces may play a role in regulating calvarial development and suture fusion [26].
Moreover, sutures and fontanels play a crucial role in enabling the infant skull to withstand mechanical impacts [33]. Rich in collagen, these structures possess the flexibility and elasticity necessary to absorb shocks, such as those resulting from falls, thereby safeguarding the developing brain.

2.4.2 Force springs

Springs serve as devices for storing potential energy due to their ability to stretch and exhibit elasticity. The physical principle behind describes the force F exerted

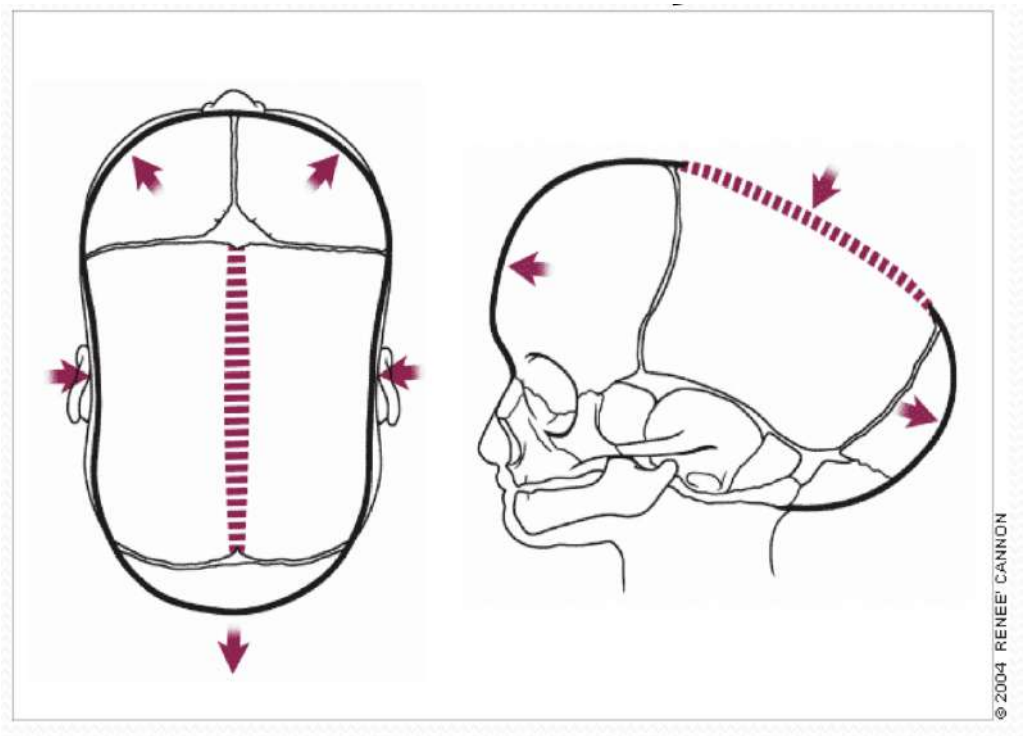

Figure 2.6: Forces acting when sagittal craniosynostosis is present, with permission from ref. [5]

Figure 2.7: forces on head, modified with permission from ref.[30]

on a body and is called the Hookean law [34]. Springs utilized in craniosynostosis surgeries adhere to Hooke's law, as represented by Equation 2.1, wherein the force is directly proportional to the level of tension or compression. Spring equilibrium

occurs when the spring reaches its natural state, meaning it is not compressed nor stretched [10, 25, 34].

$$F = -kx \tag{2.1}$$

where:

F = Force [N]
k = Spring constant [N/m]
x = amount by which the spring was displaced from its "relaxed" position [m]

Moreover, this equation 2.1 shows that the applied force to the spring is equal and opposite to the force exerted by the spring, implying Newton's third law; for every action, there is an equal and opposite reaction.

During surgery, surgeons compress the spring to facilitate insertion, generating an outward force acting as a distractor between skull plates. This outward force is directly proportional to the distance of spring opening, see Fig.2.5. Finite element method predictions of residual forces were made at intervals of 3, 6, and 9 months, resulting in forces of 8N, 6.7N, and 5.7N respectively [10], that can be take as a benchmark to follow.
In some cases, such as those in Göteborg, surgeons manually bend the springs to achieve similar outcomes, as this approach allows for better adaptation to individual patient needs and is cost-effective compared to certified manufactured springs (Professor Lars Kölby, Department of Plastic Surgery at Sahlgrenska, personal communication, January 15, 2024). Typically, the inserted springs exert a force of approximately 8N initially and gradually decrease over time [35].

While hand-bent springs offer the advantage of customization to patient characteristics and age, standardized springs are also commonly used due to their simplicity and reliability. However, studies often report the force exerted upon insertion of the springs, with limited information available regarding the rate of force dissipation over time during spring opening in vivo [35].
To address this, a collaborative effort between the Great Ormond Street Hospital for Children (GOSH) in London, UK, and the Active Spring Company (Sibleys Green, Thaxted, Essex, UK.) led to the design of a standardized torsional spring with a helix (see Fig. 2.8) to improve elastic recoil. Utilizing surgical-grade stainless steel wire, these springs were mechanically characterized to assess their force-to-opening behavior [35].

2.5 Alternative Methods

To minimize the need for surgery and improve outcomes, various strategies are being explored. One approach is to develop biodegradable springs, potentially reducing their impact on the body. Since these springs can remain in the head for extended periods, they should exert less distracting force while maintaining strong shape memory. Ultimately, the goal is to eliminate the need for surgery altogether. Research

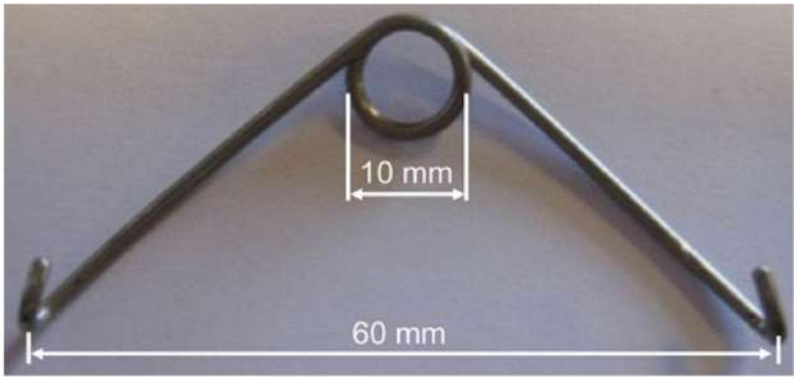

Figure 2.8: GOSH spring in relaxed state, manufactures by the Active Spring Company, with permission from [35]

efforts are focused on understanding the underlying causes of craniosynostosis and preventing its development [38].

The etiology of nonsyndromic craniosynostosis still needs to be deciphered meaning that there is no molecular target that could be genetically or pharmacologically tackled, whereas by now it is known that FGFR1-3 and TWIST1 (single gene mutations) are responsible for more than 3/4 of the most commonly encountered craniofacial syndromes. The cause for nonsyndromic craniosynostosis is likely to be multifactorial involving genetic and environmental components [39, 40].

Regarding research on novel techniques to replace the spring or any findings improving could not be found to the best of my knowledge. The trend seems to move towards finding the reason for craniosynostosis in gene and mesenchymal stem cells (MSCs) treatment so that it can be avoided before it developes [43].

Yu et al. (2021) developed a method to prevent re-synostosis and ensure long-term quality of life. They found that prior to coronal suture fusion in mice, there's a loss of Gli1+ cells, essential MSC sources in cranial sutures. They developed a modified gelatin scaffold that supports suture regeneration and implanted it with MSCs, providing a less invasive and sustainable solution [45].

Bariana et al. (2019) focused on inhibiting bone formation using protein-releasing Titania nanotubular implants (TNT/Ti) loaded with glypican 3 (GPC3) protein. This approach aims to prevent re-synostosis and has been tested in mice [46].

Faller et. al.,2015[9] tried to replace the stainless steel springs with a bioabsorbable material blend composed of PLGA and polyisoprene, tested for cranial expantion in rabbits. Although the springs showed linear expansion over time, their tensile strength varied [9].

Similarly, Marques et al. (2013) investigated using spiral stents instead of springs, incorporating cells to enhance their effectiveness [52].

These studies highlight the diverse approaches being explored to improve treatment outcomes and efforts to reduce the need for invasive surgery in patients with craniosynostosis.

2.6 Materials

Given the well-known properties of polylactic acid (PLA) in 3D printing, it was initially chosen to create a spaceholder. Although PLA is biocompatible, biodegradable, and strong, it is also brittle and rigid [27]. Surgeons emphasized the need for material expansion, strength, and biodegradation. To address these needs, I explored blends that are strong yet less brittle than PLA. After a literature review, we selected a PLA/PCL blend [8].
The PLA/PCL blends were studied with the goals of a) reducing brittleness and b) enhancing flexibility. The blend is expected to decrease overall strength while significantly increasing flexibility compared to pure PLA [8].

PLGA/PI 60:40 w/w blend also caught my attention, particularly given the promising results of ongoing animal tests conducted on rabbits. This method closely aligns with the objectives I aim to achieve, and it represents the closest approach I've encountered in the literature [9].
I also used the PLGA/PI 60:40 w/w blend because of its promising data from rabbit studies and its enhanced elasticity. This method closely aligns with the objectives I aim to achieve and represents the closest approach I've encountered in the literature [9].
PLA as well as PLGA are biocompatible and biodegradable, making them attractive for biomedical applications [37]. Their chemical structure differ and therefore their mechanical properties [36]. Generally, PLGA is more flexible and ductile compared to the stronger and more brittle PLA, due to the PGA [36].

2.6.1 PLA

PLA, a polymer made of lactic acid monomers, see Fig.2.9, is well-known for its use in biomedical applications due to its bioabsorption and thermoplastic behavior. It's particularly successful in 3D printing because of its low melting point, which makes it easy to process. PLA can be either amorphous or semi-crystalline, depending on its structure [70, 71].

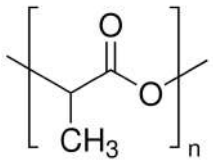

Figure 2.9: PLA composition

In the body, PLA primarily degrades through hydrolysis, where water breaks down the ester linkages in the polymer backbone. The cleavage of ester linkages results in carboxyl and hydroxyl linear polymers or oligomers with shorter chain lengths. This is followed by absorption through metabolic pathways and eventually being eliminated from the body by release of CO_2 back into the atmosphere, but this process is generally slow. High crystallinity in PLA can slow down degradation because crystalline regions are more resistant to water [69, 70, 75]. The rate of hydrolysis further depends on the water content available and the technique used to process the samples [74].
To speed up degradation, a lower molecular weight of PLA is preferred. Making PLA more hydrophilic also helps it degrade faster. For example, poly(d,l-lactic acid) (PDLLA) degrades quicker than L-lactic acid (LLA) because it has fewer crystalline regions and is more hydrophilic. The rate of PLA degradation depends on factors like molecular weight, crystallinity, morphology, and how quickly water can penetrate it.
Typically, PLA stays in the body for about 3-5 years due to its slow degradation rate. PLA also has mechanical limitations; it is brittle and has poor toughness, breaking with less than 10% elongation [71].

2.6.2 PLGA

PLGA is a copolymer consisting of lactic and glycolic acids, as depicted in Fig.2.10. Both the 50:50 and 75:25 PLGA formulations utilized in the experiments are in an amorphous state [59].

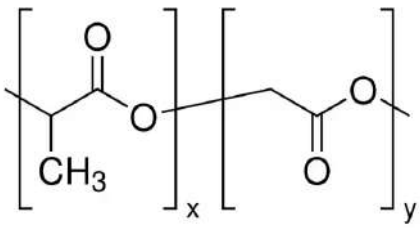

Figure 2.10: PLGA composion, left lactide and right glycolide

The degradation of the polymer primarily occurs through hydrolysis, resulting in the breakdown of lactic and glycolic acids [57]. It has been observed that degradation proceeds more rapidly in the presence of higher concentrations of glycolic acid due to its hydrophilicity [58]. For instance, the biodegradation time of DL-PLGA 75:25 is reported to be 4-5 months, while DL-PLGA 50:50 degrades within 1-2 months [63].
Degradation initiates with the hydrolysis of the ester bonds and can occur through bulk or heterogeneous erosion mechanisms [58]. The methyl side in the lactic acid moiety imparts greater hydrophobicity compared to the glycolic acid moiety, rendering these copolymers less hydrophilic and more prone to degradation via hydrolysis [59]. Upon immersion in aqueous media, PLGA samples exhibit swelling and wrinkling of the surface [57].

Additionally, a higher content of lactic acid corresponds to a higher glass transition temperature (Tg), and the increased hydrophobicity results in slower diffusion of water or aqueous media, thereby decelerating the overall degradation process [57]. The broken-down lactic acid is metabolized in the tricarboxylic acid cycle and excreted via carbon dioxide and water. In contrast, glycolic acid undergoes metabolism in the tricarboxylic acid cycle but is excreted through the kidneys. Moreover, glycolic acid can be further metabolized into oxalic acid, potentially leading to systemic toxicity during PLGA implantation or prolonged circulation within the body [59]. The ratio of PLA and PGA not only influences the degradation rate of the polymer but also affects its crystallinity, mechanical properties, and size [61].

PLGA is available in various molecular weights (Mw), and selecting the appropriate one is crucial for the functionality of the blend. Higher Mw within the same polymer results in greater resistance towards degradation of force, and higher viscosity as melt. PLGA with a high Mw possesses longer chains, facilitating easier entanglement, thereby enhancing its mechanical strength and ductility, whereas lower Mw tends to render the polymer more brittle due to the chains being more susceptible to separation [60].

2.6.3 Polyisoprene

Polyisoprene, also known as natural rubber, is a polymer composed of repeating isoprene subunits that form a long chainlike molecule. It is synthesized through a series of biochemical reactions originating from isopentenyl pyrophosphate within the tree, as depicted in Fig. 2.11.

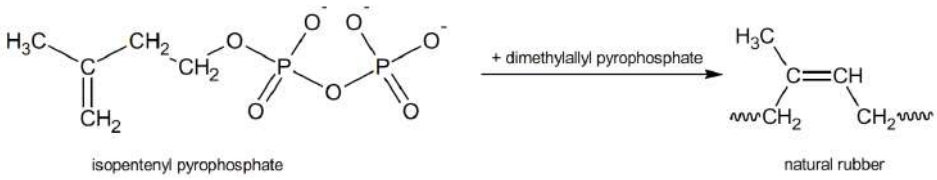

Figure 2.11: Biochemical reaction for natural rubber

Natural rubber typically exists in a cis-1,4 configuration, meaning that the 1 and 4 carbon atoms are attached to the same side of the carbon-carbon double bond. When polymer chain units are arranged regularly in space, interactions such as polar attraction, hydrogen bonding, or functional groups can lead to the formation of crystalline structures, thereby stiffening the polymer. Crystallites can form in natural rubber upon storage and stretching. The natural rubber available on the market, comprises approximately 94% polyisoprene with a cis-1,4 configuration. The remaining 6% consists of non-rubber constituents, including approximately 2.2% proteins, 3.4% lipids (fatty acids, glycolipids, and phospholipids), and 0.4% carbohydrates [55]. There is also a synthetic rubber, where the non-isoprenic compounds do not exist [64].
The presence of carbon-carbon double bonds and hydrocarbon atoms limits the miscibility of cis-1,4-polyisoprene. To address this issue, chemical modifications of poly-

isoprene are explored, focusing on altering the internal structure through processes such as epoxidation. Opening the double bonds forms epoxy groups, increasing the polarity of polyisoprene and enhancing its compatibility with PLGA [56].
Marques (2011) indicates that PI is a non-absorbable polymer, thus it is not incorporated into recipient tissue and is eliminated from tissue contact within approximately 15 days. Faller et al. (2015) suggests that the bioabsorption of polyisoprene occurs via a metabolic pathway. Another study demonstrated the integration of polyisoprene with bone [62].

2.7 Shapes and Patterns for 3D print

For the PLA 3-D prints I opted for a cylindrical form. The circular base, being one of the strongest structural shapes, ensures even stress distribution along the arc, avoiding concentration at specific points. Consequently, the cylinder was chosen. While a fully filled cylinder is the strongest, considering the importance of degradation for 'resorbable springs', I chose a grid and honeycomb infill due to the printers limitations of choosing patterns with different percentages of infill to see which ratio is best. The infill not only reinforces the structure of a hollow cylinder but also adds a faster degradation to the otherwise plain cylinder.
The material blends will be hand molded in a cuboid shape, not only because of simplicity but also following the literature [9].

2.8 Biodegradation

Polymers can be categorized into hydrophilic and hydrophobic types. PLA, PGA, and their copolymer, PLGA, fall into the hydrophobic category. Enzymatic or nonenzymatic hydrolysis cleaves their polymeric chains throughout the matrix, resulting in bulk erosion [50]. The resultant products, such as PLA and PGA, are metabolized through the Krebs cycle to carbon dioxide and water [47].

To simulate the fluid environment of the human body post-surgery, typically, simulated body fluid (SBF) is used, mimicking blood plasma [49]. To accurately replicate the brain's fluid environment, both CSF and blood circulation need to be simulated. The fluid volume in infants is estimated to be between 11 and 15 ml per kg of body weight. It is thought that approximately 50% of this volume is located in the spinal canal, decreasing with age, resulting in a cranial volume of about 5 to 10 ml per kg of body weight in infants [72]. SBF is an acellular, protein-free, supersaturated calcium-phosphate solution with an ionic composition similar to human blood plasma and CSF and is generally buffered at physiological conditions (pH 7.4 and 36.5°C) [49].

While SBF contains Mg^{2+}, Ca^{2+}, and HCO_3^-, phosphate-buffered saline (PBS) does not (see Tab.2.12). However, since our focus is on aqueous hydrolysis of polymers, PBS suffices [48]. PBS with fewer ionic constituents results in fewer apatite crystals compared to SBF [50].

According to Hooper et al. (1998), the in vitro degradation of poly(L-lactic acid) (PLLA) varies with surface roughness. While PBS does not cause noticeable changes in surface roughness, SBF leads to increased blistering on the implant's surface. Additionally, PLLA exhibits a water uptake of 20-30% in PBS within a short period, whereas in SBF, it reaches up to 50% [51].

The pH of the solvent is crucial during sample degradation as it determines the degradation rate. The more acidic the pH, the faster the degradation.
Wound pH varies depending on the type of wound, but generally, a pH of 7.4 is mentioned. Conversely, the human epidermal layer has a slightly acidic milieu, with a pH range of 4.5–5.3 [53].

Type	Ion concentration (mM)						
	Na^+	K^+	Mg^{2+}	Ca^{2+}	Cl^-	HCO_3^-	HPO_4^{2-}
Blood plasma	142.0	5.0	1.5	2.5	103.0	27.0	1.0
SBF	142.0	5.0	1.5	2.5	148.8	4.2	1.0
PBS	157.0	4.5	–	–	140.0	–	10.0

Figure 2.12: Composition of blood plasma, SBF and PBS [48]

3
Methods

This section details hand-molding techniques alongside with the methodology employed for printing the PLA samples. It further outlines the methods utilized to assess the strength properties and degradation of the samples.

3.1 Blends

Blend samples were manufactured using a blend of bioabsorbable PLGA/PI copolymer, as well as PLA/PCL.
Various types of PLGA were evaluated for optimal performance. PLGA, a copolymer comprising 50 mol% monomer L-lactate and 50 mol% glycolide with a Mw ranging from 38,000 to 54,000 g/mol, was procured from Sigma Aldrich (Germany) and used without further purification. Additionally, PLGA with proportions of 50 mol% monomer L-lactate and 50 mol% glycolide, ester terminated, and a Mw of 7,000 to 17,000 g/mol was acquired from Sigma Aldrich (Germany) for comparison. Furthermore, PLGA Poly(D,L-lactide-co-glycolide) with a lactide:glycolide ratio of 75:25 and a Mw of 66,000-107,000 g/mol was obtained from Sigma Aldrich.
Cis-1,4-Poly(Isoprene) (PI) with a Mw 38,000 g/mol, derived from natural rubber and purchased from Sigma Aldrich (Germany), was utilized.
PLA with a Mw of ∼60,000 g/mol was sourced from Sigma Aldrich (Germany) and used without additional purification.
Polycaprolactone (PCL) with a relative molar mass Mr of ∼10,000 g/mol was obtained from Fluka (Germany).

Blends of PLGA/PI and PLA/PCL were prepared in various mass proportions: 90% PCL/10% PLA, 80% PCL/20% PLA, 70% PCL/30% PLA, 60% PCL/40% PLA, and 50% PCL/50% PLA. Similarly, PLGA/PI blends were prepared in the following ratios: 90% PLGA/10% PI, 80% PLGA/20% PI, 70% PLGA/30% PI, and 60% PLGA/40% PI.
To address the stiffness of the PLA/PCL samples, 10% PI was added.

Glass vials with a 1.2cm diameter were utilized. PI was weighed into the vials, followed by the addition of PLGA for PLGA/PI blends and PLA and PCL for the PLA/PCL samples. Chloroform was then added to dissolve the components, and all samples were manually mixed with a metal spatula. During the initial day, the samples were stirred approximately 5-6 more times to prevent separation. Once dried after approximately 1 day, the samples were removed from the vial using tweezers.

Subsequently, the samples were stirred using a magnetic stirring plate to ensure thorough mixing.
A table of the different PLGA and PLA that has been used in the experiment can be seen in Tab. 3.1.

Table 3.1: Used PLA and PLGA to conduct experiments

Material	Mw
PLGA (50:50), ester terminated	7,000
PLGA (50:50)	38,000 - 54,000
PLA	ca. 60,000
PLGA lactide:glycolide (75:25)	66,000 - 107,000

3.2 3D printing

Prior to initiating the 3D printing process, a cylindrical model measuring 2 cm in diameter and 4 cm in height was crafted using Fusion 360. Subsequently, it was exported as an STL file to Voxelizer. Within Voxelizer, infill patterns including "light" with 10% infill, "light honeycomb" with 10% infill, and "medium" with 30% infill were selected, as illustrated in Fig. 3.1. Additionally, a Power raft was chosen for the bottom layer. These three models were then exported to the ZMorph VX 3D printer via an SD card.

The printer's nozzle diameter was set at 0.3 mm. Manual calibration of the printer was performed, and the print bed was preheated to 60°C. The nozzle temperature was set to 210°C, and nine samples of each model were printed. The filament utilized was the pearl red PLA with a diameter of 1.75 mm, sourced from ZMorph FILAMENTS.

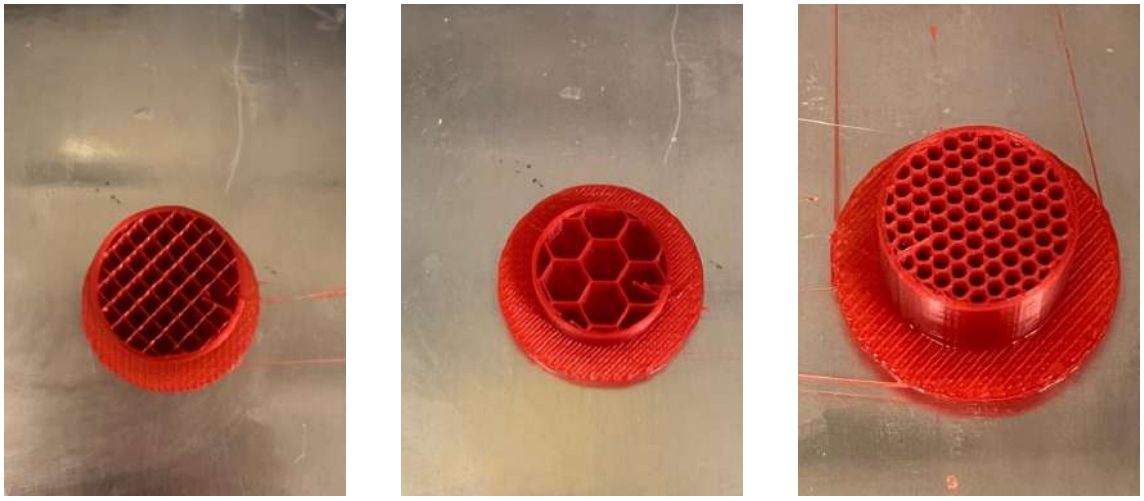

(a) "light" **(b)** "light honeycomb" **(c)** "medium"

Figure 3.1: Different infill patterns for cylindrical samples with ⌀ 2 cm and a height of 4 cm

3.3 Mechanical testing

Before conducting the mechanical testing, all 3D printed samples underwent weighing using the Sartorius Analytical Balance CP224S precision scale. From each batch, the initial five 3D printed samples were selected for the mechanical testing.
For the mechanical testing, the Instron 5565A Mechanical Tester was used. A 5 kN load cell was utilized to measure compressive force at a consistent rate of 5 mm/min. Compression testing was halted either when the sample reached 50% compression or when the load cell registered a force of 4 kN, see Fig.3.2.
The resultant stress-strain curve for each specimen was analyzed to determine the applied force and the extension of each sample, as depicted in Figs. 4.1 and 4.2.

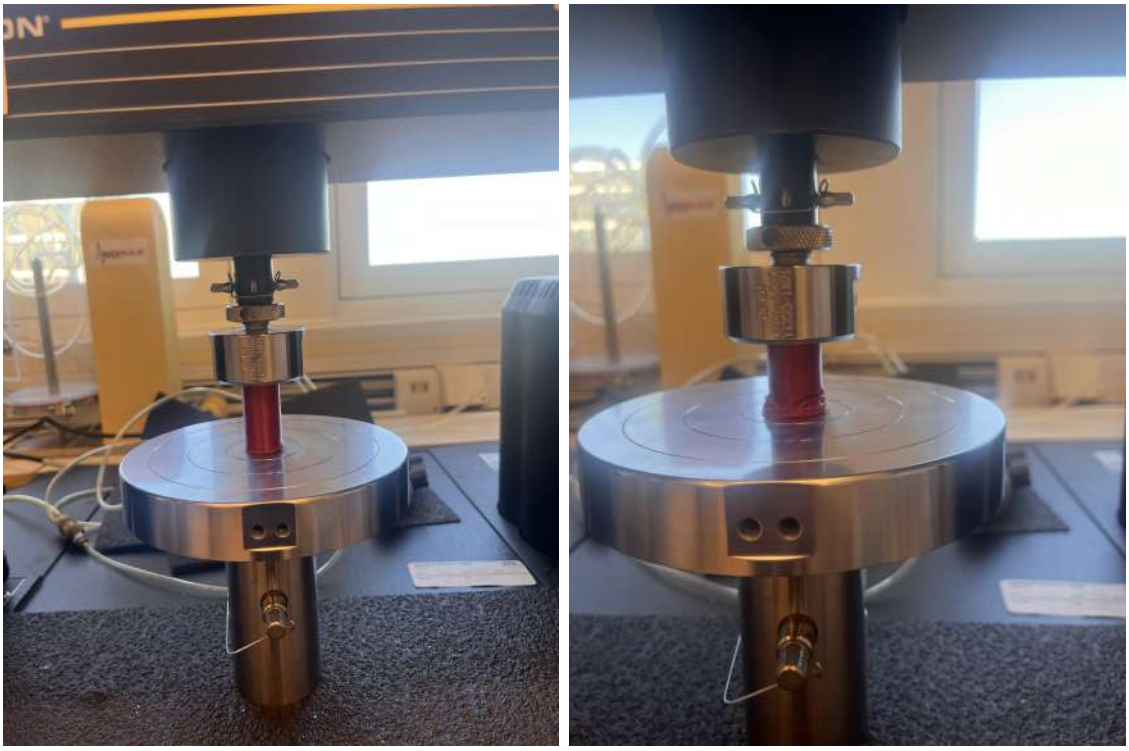

Figure 3.2: PLA sample in the mechanical tester while putting force on it

3.4 Degradation

The natural in vitro degradation experiment was conducted using phosphate-buffered saline (PBS) at two distinct pH levels: pH 7.4 and pH 5. pH 5 was achieved by introducing hydrochloric acid (HCl) into the solution. The 3D printed samples, along with PLGA/PI blends at ratios of 80:20 and 90:10, were immersed in 600 ml of the respective PBS solutions.
A Prolabo dissolution instrument equipped with paddles (refer to Fig. 3.3) was utilized in conjunction with a water bath maintained at a constant temperature of 37°C. However, the Prolabo dissolution instrument encountered difficulty in maintaining the desired temperature, resulting in fluctuations between 24-43°C.
The same experimental setup was used for the PLGA/PI samples, with the addition

of a basket alongside the paddles to secure the samples in place.
The materials underwent biodegradation for a duration of 46 days for the PLA samples and 38 days for the PLGA/PI samples, with stirring set at a speed of 100 rpm. Each day, the samples were weighed while wet, and the pH of the PBS was monitored to ensure consistency throughout the experiment.

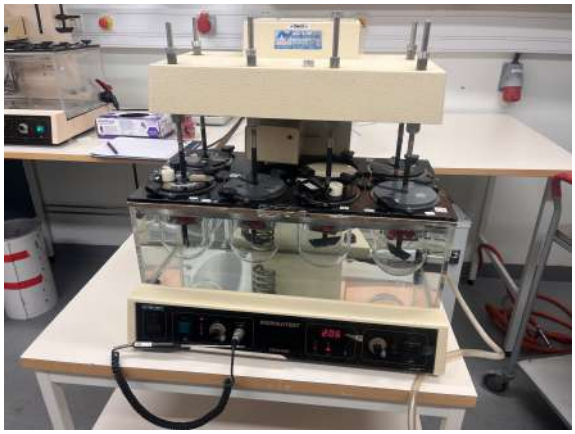

Figure 3.3: Dissolution bath for PLA samples

3.5 Hot manual press

The PLGA/PI samples were prepared by positioning them within a mold and enclosing both sides with appropriate plastic coverings. The press, depicted in Fig. 3.4, was initially heated to 160°C, followed by subsequent temperature adjustments to 190°C and 210°C, each maintained for one minute. Following this, a force of 50 kN was exerted on the samples and sustained for an additional 3 minutes. Upon completion, the samples were delicately extracted from the press and left to cool.

Figure 3.4: Manual press

4

Results and Discussion

In this chapter the different results as well as the discussion for the different parts of the project are presented.

4.1 Axial compression testing of 3D-printed samples

Compression testing was conducted on the 3D printed PLA samples to analyze their behavior under an applied quasi-static crushing load. Throughout the testing process, the Young's modulus and yield strength were determined, and compressive stress-strain curves were generated, as illustrated in Figs. 4.1 and 4.2.
For the purpose of this project, the maximum force endured before sample failure was of particular interest, as the samples were expected to withstand forces comparable to those exerted on the skull. Analysis of the collected data revealed the average maximum loads of the "light" and the "light honeycomb" samples with 2109 N and 3000 N respectively, together with their standard deviations of 142 N and 88 N, see Fig.4.3.
This suggests a more consistent print with less variability in the honeycomb-shaped samples compared to the grid-shaped ones.
Upon comparison of the compressive stress-strain curves obtained from the two types of samples (Figs. 4.1 and 4.2), it can be observed that the "light" samples

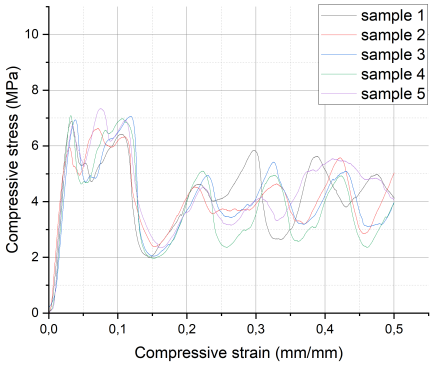

Figure 4.1: Compression stress-strain graph for "light" samples

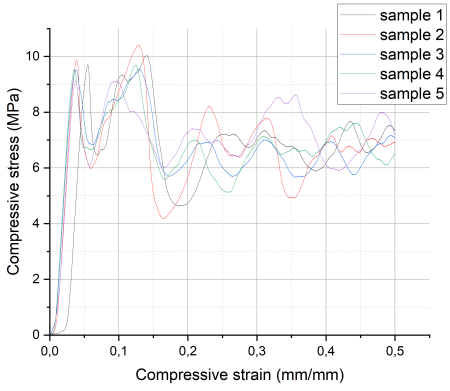

Figure 4.2: Compression stress-strain graph for "light honeycomb" samples

exhibit three higher peaks in the range of 6.5 to 7.5 MPa, whereas the "light honeycomb" samples display two major peaks in the range of 9 to 10 MPa. This implies that graphically, the "light" samples possess more "strong points" before experiencing significant deformation, whereas the "light honeycomb" samples exhibit greater ductility, as evidenced by the more spread out high peaks and smaller fluctuations in the stress-strain curves.
However, for the "medium" samples (measuring 2 cm in diameter and 4 cm in height), no maximum values could be measured due to limitations with the size of the load cell. Nonetheless, it was inferred that these samples could withstand forces exceeding 10 kN.

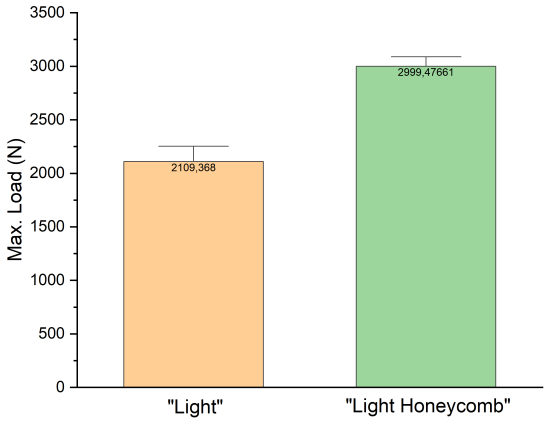

Figure 4.3: Maximum loads and standard deviations

Upon examination of the stress-strain curves, a distinct failure is evident, characterized by multiple peaks and valleys, indicating instances where the samples yielded to increased force after reaching the initial valley.
In an ideally printed PLA sample, the failure would occur a bit later. However, as illustrated in Fig. 3.1, smaller printing errors occurred throughout the samples randomly, contributing to an earlier failure mode.
This cyclic behavior is illustrated in Fig. 4.4, where the bulging signifies the buckling and rupture of the sample in the graphs. Notably, the intensity of buckling in the honeycomb structure is less pronounced compared to the grid pattern, as observed in Fig. 4.1 and Fig. 4.2, suggesting that the honeycomb structure can withstand

Figure 4.4: Buldging of sample

higher forces compared to the grid pattern infill.
Furthermore, observed deformation initiates with the buckling of cell walls, followed by localized shearing, leading to progressive collapse, starting from the bottom.
Another notable finding is that in both graphs, the first two to three peaks are roughly of the same height, whereas subsequent peaks decrease. The bulging of the samples occurs uniformly at the bottom and gradually progresses upward, a natural behavior attributed to the increased load-bearing requirements at the bottom. This results in local buckling of the infill and eventual gradual failure of the PLA sample, explaining the prolonged fluctuation of applied load.
Furthermore, the results indicate that the structural integrity remains intact during the initial linear stage of compression loading, demonstrating an exceptionally high load-bearing capacity. For this project, emphasis is placed on the linear stage of compression, as the space-holder samples are intended to maintain their shape over their lifespan, making elastic deformation more pertinent than plastic deformation. The maximum stress a sample can withstand without undergoing plastic deformation, known as the yield strength practical approximation of the elastic limit, was determined to be 6.7 MPa for the "light" samples and 9.6 MPa for the "light honeycomb" samples. A comparison between the two sample types reveals that the "light honeycomb" samples exhibit higher resistance to compressive strain, indicative of their ability to withstand greater applied force without deforming. This observation is further supported by the mean Young's moduli of the samples. The "light" samples have a mean Young's modulus of 325 MPa with a standard deviation of 21 MPa, while the "light honeycomb" samples have a mean Young's modulus of 402 MPa with a standard deviation of 12 MPa.
Additionally, the slight delay observed in the black curve in Fig. 4.2 is attributed to a manual error during sample placement, resulting from the positioning of the load cell.
Considering the layer-by-layer printing process of the 3D samples, directional properties vary within the samples. However, pure PLA exhibits excessive strength for practical use, necessitating scaling down of all values by a factor of 4 to fit the dimensions of the skull. The Table 4.1 therefore indicates the average force per weight ratio of the different samples.For the intended purpose of using PLA spaceholders as replacements for stainless steel springs, it can be concluded that the "light" grid infill provides more than sufficient strength.
Moreover, the amount of material used, indicated by higher infill, correlates with increased load-bearing capacity, highlighting the interplay between infill density and load-bearing capacity.

Table 4.1: Average loads and weights of 3D printed PLA constructs

Pattern	Average max load (N)	Average weight (g)	Average α (N/g)
light	2110	3.7	600
light honeycomb	3000	3.9	750
honeycomb	>10.000	6.2	>1600

The objective of this experiment was to ascertain the optimal infill pattern in terms of maximum load-bearing capacity while minimizing weight. The average maximum

load weight ratio (α) is computed by dividing the average maximum load by the weight of the infill pattern as follows:

$$\alpha = \frac{\text{average max. load}}{\text{average weight}} \tag{4.1}$$

4.2 Blend results

Following the approach outlined by Faller et al. (2015) that I got inspired of, I experimented with various combinations of PLGA and PI to identify the most suitable blend for replacing stainless steel springs. To meet the requirements, the samples should:

- Not be sticky
- Maintain their molded shape
- Ideally behave like a spring when touched and bent

Different blends and compositions were therefore tested and evaluated, as summarized in Table 4.2.

Table 4.2: Various PLGA/PI and PLA/PCL blends

Sample Type	**Mw**	**Ratio (w/w)**	**Meet requirements**
PLGA (50:50), ester terminated	7,000	60:40	no
		70:30	no
		80:20	no
		90:10	no
PLGA (50:50)	38,000-54,000	60:40	no
		70:30	no
		80:20	no
		90:10	no
PLGA lactide:glycolide (75:25)	66,000-107,000	60:40	no
		70:30	yes
		80:20	yes
		90:10	yes
PLA	ca. 60,000	40:60	no
		30:70	no
		20:80	no
		10:90	no
PLA/PCL + 10% PI	ca. 60,000	40:60	no
		30:70	no
		20:80	no
		10:90	no

4.2.1 Evaluation

In Table 4.2, it is evident that only samples containing PLGA with a high Mw were able to achieve a non-sticky consistency. This outcome was anticipated, as longer PLGA chains tend to entangle more easily and can initially entrap more phase of PI compared to shorter chains.
Observing the Table 4.2, PLGAs with a Mw of 7,000 g/mol and 38,00-54,000 g/-mol exhibit a lactide/glycolide ratio of 50:50, whereas the effective PLGA with a Mw of 66,000-107,000 g/mol possesses a ratio of 75:25. The varying ratios affect the shape, degradation rate, melt viscosity, and resistance of the polymers. Upon blending the mixture, a more viscous behavior was noted in the PLGA with a Mw of 66,000-107,000 g/mol.
It also demonstrates that PLGA/PI ratios of 70:30, 80:20, and 90:10 yielded optimal results, indicating that a higher proportion of PLGA is necessary if its molar mass is lower than that reported in the literature [9] to achieve comparable outcomes. Consequently, shorter chains may have limited capacity to trap the PI phase. While the 70:30 ratio exhibited slight phase separation that resulted in stickiness, I opted to focus solely on the 80:20 and 90:10 ratios. Despite the reduced amount of PI in the samples compared to the 60:40 ratio reported in the literature, there appears to be no noticeable impact on the flexibility of the samples, all of which displayed remarkably good flexibility. This shows a more flexible behaviour of PLGA with lower Mw compared to the PLGA with longer Mw that is used in literature. However, in the 90:10 ratio, a slightly diminished ability to "bounce back to the initial shape," was observed, leading to the selection of the 80:20 blend.

In parallel I explored another blend composition comprising PLA and PCL, as illustrated in Tab.4.2.

This blend proved to be extremely brittle across all ratios. Upon handling the blend, it began to crumble. One potential factor contributing to this outcome could be the PLA, as its molecular weight was approximately 60,000, whereas the successful PLGA blend had a higher Mw.
Furthermore, crystallinity in a polymer leads to increased brittleness and strength. In contrast, amorphous regions in polymers gives them toughness. The PLGAs used in the experiments were all in an amorphous state, providing the toughness, and flexibility which are desired attributes [59, 70].

Figure 4.5: left: PLGA(Mw7,000)/PI blend 60:40 (w/w), right: PLGA(Mw 38,000 - 54,000)/PI blend 60:40 (w/w)

In the future, exploring the blending of PCL with PLGA could be considered.
Figure 4.5 displays two blends with varying lengths of PLGA, where the dark brown

PI layer is visibly positioned on top of the PLGA. This observation indicates phase separation, and upon tactile examination, I noted the stickiness of the samples due to the high viscosity of PI.

After attempting to reconstruct the samples following the methodology described in other papers [9, 52], utilizing a w/w ratio of 60:40, as depicted in Figure 4.5, the results showed phase separation. To further investigate this issue, a comprehensive series of experiments was conducted using various ratios of the two PLGAs, as outlined in Table 4.2. Upon air drying the samples, consistent phase separation and stickiness were observed across all ratios. However, a slightly reduced stickiness was noted in the samples containing PLGA with Mw ranging from 38,000 to 54,000 g/mol compared to those with PLGA of Mw 7,000 g/mol. This implies that longer PLGA chains play a role in decreasing the stickiness of the samples. Longer chains are more likely to entangle, potentially trapping more PI within them. However, due to the density differences between the two materials—0.92 g/mL at 25°C for PI and 0.26 g/cm3 at 25°C for PLGA—they will eventually separate.

I successfully obtained samples as depicted in Figure 4.6. However, the vials utilized were bulged at the bottom and therefore not flat at the bottom, resulting in uneven shaping of the samples. Consequently, they were not suitable for conducting a mechanical compression test to assess their ability to withstand a force of 8 N.

Figure 4.6: PLGA/PI blend 90:10, 80:20, 70:30 from left to right

In addition to the standard vials initially employed, as shown in Fig. 4.6, various molds made from different materials were tested to produce samples suitable for testing (depicted in Figs. 4.7a, 4.7b, 4.7c and 4.7d).

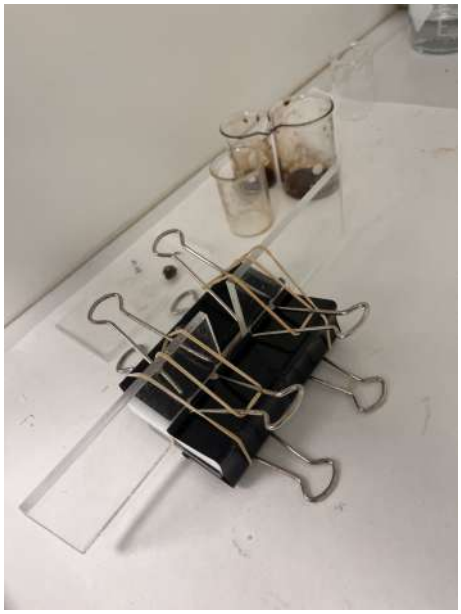

(a) Mold made out of glas and plexiglas

(b) Result from a)

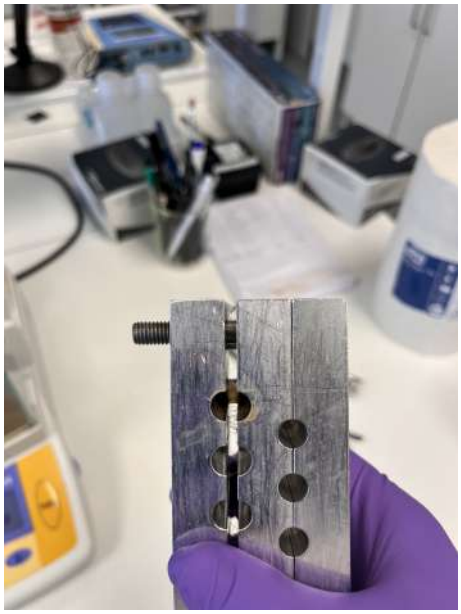

(c) Mold for suppositories made out of steel with dimensions: ∅ 0.8 cm and height of 3 cm

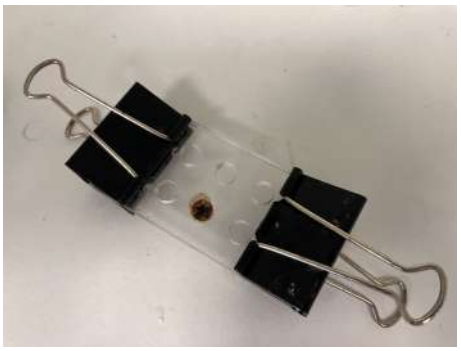

(d) Tablet mold with dimensions: ∅ 1cm, height 0.5cm

Figure 4.7: Different molds

Due to the use of chloroform, careful consideration was required in selecting the appropriate material for the mold to prevent dissolution. While glass and metal molds proved resistant, Plexiglas exhibited some dissolution, making it challenging to extract the sample. Additionally, a bigger surface aids in chloroform evaporation, resulting in faster drying and therefore less time for phase separation between the

polymers.
As the Mw of PLGA increases, a greater amount of chloroform is required for dissolution. The amount of chloroform that evaporates upon drying is more than 50% of the blends volume. Additionally, upon re-dissolving a hardened sample in chloroform, it appears that the polymers also dissolved and evaporated.
However, difficulties arose in extracting samples from molds, especially with deep molds posing a higher risk of damage of the sample during retrieval. Even molds with multiple parts proved problematic, as the liquid sample tended to leak.
To overcome these challenges and obtain testable samples, an alternative approach involved conducting tension tests. The intention was to compress the samples in a hot press to achieve uniformity. However, the issue of phase separation persisted, hindering the production of homogeneous and even samples for mechanical testing. As depicted in Fig. 4.8, despite efforts to consolidate the components, they remained separated, forming small islands and leaving behind holes, rendering the samples unusable.

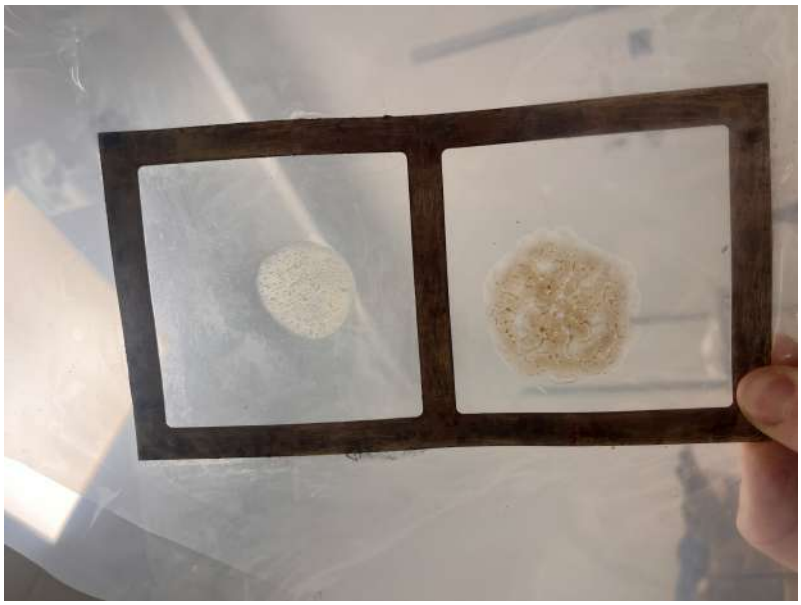

Figure 4.8: Samples after being pressed

To address immiscibility issues, the PI was cleaned with HCl and methanol following the procedure outlined in the paper by Faller et al. [9]. Another batch of PI was subjected to drying in an oven at 40°C for 24 hours. Despite these efforts, no noticeable differences were observed in the blend, meaning that the phase separation persisted.

4.2.2 Comparison with original paper

Faller et al. (2015) [9] employed the following methodology to fabricate and evaluate the implants tested in rabbits, as in Fig. 4.9.
I used this paper as inspiration but tried to mold it a bit differently:

2.3. Implants

The spring implants used in the study intervention were manufactured from a bioabsorbable poly(lactic-co-glycolic acid)/polyisoprene (PLGA/PI) copolymer blend (Jahno et al., 2007; Marques, 2011) at the Biomaterials Laboratory, UFRGS School of Engineering (LABIOMAT, Porto Alegre, Brazil).

PLGA (84 mol%:16 mol% L-lactide/glycolide monomer ratio) was obtained from Purac Biomaterials (the Netherlands) and used as supplied, without any additional purification or processing. The pH as supplied was 7.2, thus obviating the need for neutralization (Marques, 2011).

PI was obtained from Mafer Ltda (Estância Velha, Brazil) as 60% centrifuged natural rubber latex. The pH as supplied was 10.0–11.2. Therefore, the material was neutralized with 2 M HCl solution to a pH range of 7.2–7.8. Before use, the polymer was completely dried and purified by reprecipitation from chloroform into methanol. After precipitation, the material was dried again (Marques, 2011). Chloroform and methanol (both 99.8%) were obtained from Synth (São Paulo, Brazil) and used as supplied.

The springs were manufactured as follows. Briefly, solid PLGA and PI were weighed separately. The materials, at a ratio of 60% PLGA: 40% PI by mass (51% PLGA: 49% PI by volume), were dissolved in chloroform by magnetic stirring. After homogenization, the polymer/solvent mixture was dried for 72 h at 40 °C for solvent evaporation. The resulting material was injection molded at 165 °C in a HAAKE MiniJet II system (Thermo Scientific) to form necked samples (width 4 mm, length 30 mm, thickness 2 mm). These specimens were molded in distilled water at 70 °C. For mechanical characterization, all specimens underwent compression testing in an Instron 3369 universal testing machine with a 2-kN load cell. The test was performed as per ISO standard 527-1 (British Standards Institution, 1996) at LABIOMAT.

Figure 4.9: Methods part of Faller et al. (2015) with permission from ref. [9]

4.2.2.1 PLGA with lactide:glycolide (75:25), mol wt 66,000-107,000

Due to the shorter degradation time I chose a PLGA with lactide:glycolide (75:25), mol wt 66,000-107,000 rather than the PLGA (84 mol%:16 mol% L-lactide/glycolide monomer ratio).

4.2.2.2 No purification on PI

In the study, Faller utilized centrifugation, neutralization, and purification techniques on the PI. However, due to the brown color and high viscosity of the PI, I encountered difficulty in measuring its pH and consequently could not neutralize it. Further complicating matters, there appears to be ambiguity regarding the composition of the PI from different suppliers. According to the Mafer Ltda. webpage, their PI is synthetic, whereas Sigma Aldrich indicates that the PI is derived from natural rubber. While the natural rubber variant reportedly contains 94% polyisoprene with a cis-1,4 configuration, the remaining 6% consists of non-rubber constituents, including proteins, lipids, and carbohydrates [55].

The centrifugation and purification processes likely reduce the presence of non-isoprenic compounds, which may be significant if the PI is indeed of natural origin. Therefore, future investigations should explore the exact composition of both PI variants and ascertain the necessity of cleaning and neutralizing procedures.
I attempted to address these uncertainties by subjecting the PI to drying for 24 hours at 40°C and separately cleaning it with a 2 M HCl solution and methanol, where the HCl will hydrolyse the impurities. Upon blending the treated PI samples, visual and tactile inspections revealed no noticeable differences between them. Further analysis via UV-visible spectroscopy or with a scanning electron microscope is required to determine the protein amount and whether cleaning and neutralizing procedures are essential or not.

4.2.2.3 No injection molding

Faller employed a method of drying the samples in an oven for 72 hours at 40°C to allow the solvent to evaporate. In contrast, I opted for air drying, as I observed no significant difference in results. A trial where one sample was dried in the oven still resulted in phase separation, indicating that this step may not be crucial. Moreover, it appears that the PLGA/PI blend remains immiscible regardless [56], suggesting that this drying step may not be deciding.
However, injection molding could offer advantages. My samples tended to adhere to the side walls of the vials, forming thin films, which was undesirable. Additionally, the blend's high viscosity makes it challenging to mold with a pipette or similar tool, thus injection molding could prove highly beneficial in this regard. However, in terms of temperature benefits, it may not be advantageous. Attempts to hot-press the samples at 200°C were unsuccessful, while in the referenced paper, injection molding was conducted at 165°C.

4.2.3 Morphology

Phase separation and the immiscibility of the PLGA/PI blends turned out to be the largest obstacle to prepare materials from PLGA/PI blends. Because of reproducibility I wanted to get a few samples that are the same and that can be mechanically tested, but the glass vials were bulged towards the inside at the bottom, therefore the samples had uneven thickness and were not suitable for testing. Therefore, I wanted to do a tension test by hot-pressing the samples and obtain a even and thin layer that could be put on the tester. As visible to the naked eye, in Fig.4.10, the sample formed small islands, further enhancing the tendency of phase separation. The dark brown dots are the PI that is not integrated in the PLGA. With this uneven sample the tension testing was not possible.

4.2.4 Chemical structure

While PI is a homopolymer consisting of repeating isoprene units, PLGA is a copolymer composed of repeating units of lactic acid and glycolic acid. This structural difference results in distinct chemical properties compared to PI. Additionally, the

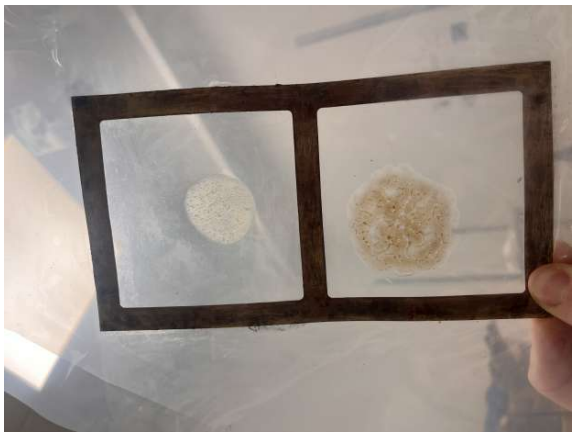

Figure 4.10: Hot pressed samples

presence of carboxyl (-COOH) groups in PLA and PLG renders PLGA more polar than the non-polar PI, potentially contributing to miscibility issues.

4.2.5 Thermodynamic properties

The miscibility of the two polymers also relies on the interplay between their enthalpy and entropy within the blend. For the mixture to achieve thermodynamic stability, the Gibbs free energy must be negative, indicating a balance between the enthalpy of mixing and the entropy of the blend.
Hydrogen bonds appear to be important in determining the miscibility of a blend, and in the case of PLGA/PI, it is possible that the hydrogen bonds are disrupted either by chloroform or mechanical mixing. This disruption of hydrogen bonds can alter the enthalpy of the system, potentially leading to immiscibility issues. Essentially, the energy required to break and form new hydrogen bonds may not be compensated by the increase in disorder when the polymers mix.

4.2.6 Different mixing methods and solvents that could be tried

Further suggestions to improve the suitability of the material include experimenting with different blending techniques, such as melt blending, possibly in conjunction with injection molding or freeze drying [65].
Alternatively, investigating the dissolution of polymers in alternative solvents, such as tetrahydrofuran (THF) and hexafluoroisopropanol (HFIP), could present viable solutions [66, 67].
According to the NFPA (National Fire Protection Association) 704: Standard System for the Identification of the Hazards of Materials for Emergency Response, chloroform and THF are classified as hazardous to health, while HFIP is considered an extreme health hazard. In terms of flammability, chloroform and HFIP are non-flammable, whereas THF is flammable below 37°C, which would limit drying methods for the samples. Regarding stability, HFIP is stable, but chloroform and THF are unstable when heated. This suggests that chloroform is the easiest

to handle of the three, followed by HFIP due to its non-flammable nature. Another significant consideration is cost, with chloroform being the most economical option, followed by THF at a slightly higher cost, while HFIP is considerably more expensive.

4.3 Degradation

In this section the degradation of all samples will be discussed. PBS solutions with pH 7.4 and pH 5 respectively, were chosen, based on findings from Hooper et al. (1998) [51], which indicate that PLA samples absorb 20-30% of their weight in PBS, compared to 50% in SBF. Additionally, the water uptake by PLA samples occurs more rapidly in PBS than in SBF. These two factors make PBS a more practical choice for degrading the samples.

4.3.1 Degradation PLA samples

The objective of this experiment was to assess whether different infill patterns influence the degradation rate of PLA samples.
In Figs.4.11 - 4.13 the wet weights of the samples can be seen in the time-period of 46 days.

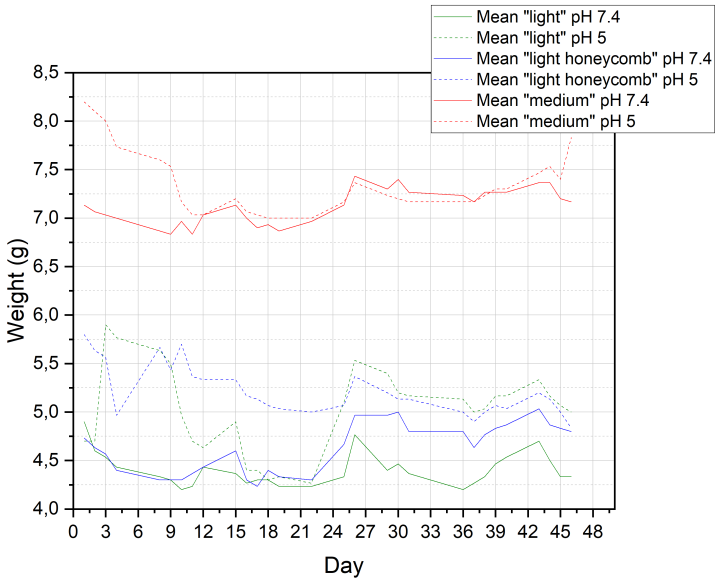

Figure 4.11: Mean degradation of PLA samples

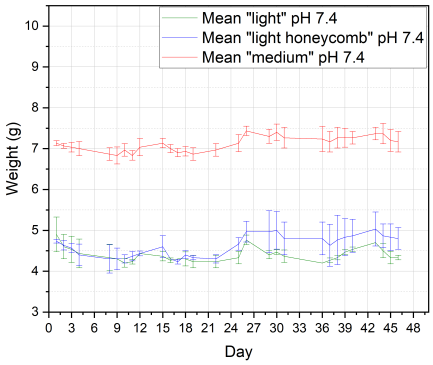

Figure 4.12: Mean degradation of PLA samples in PBS solution with pH 7.4 and standard deviations

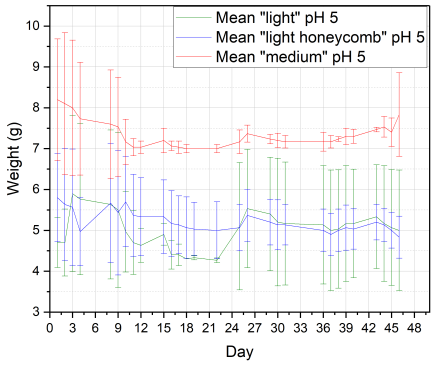

Figure 4.13: Mean degradation of PLA samples in PBS solution with pH 5 and standard deviations

As anticipated, during the initial month, the cylindrical samples with a diameter of 2 cm and a height of 4 cm exhibited relatively stable values in both PBS solutions, at pH 7.4 and pH 5. Some samples showed a higher water uptake than the other samples, possibly due to printing errors on their surfaces, facilitating water penetration.
Overall, the degradation curves showed a slight downward trend, although not significant. No observable changes in the shape of the samples were noted, except for some swelling at the bottom or top in slightly damaged samples. Additionally, there were no noticeable differences in the samples shapes between samples exposed to pH 7.4 and pH 5 solutions.

Table 4.3: Areas under the curves and dry weights of different PLA groups

Group	Average dry weight (g)	Area under the curve	Average area under the curve	Standard deviation of area under curve	pH level and consistency note
C1	3.7	120 120 125	120	3	pH 7.4, consistent
C2	3.7	125 120 170	140	29	pH 5, less consistent
C3	3.8	120 130 130	130	6	pH 7.4, consistent
C4	3.8	160 130	145	16	pH 5, less consistent

Continued on next page

Table 4.3 – *Continued from previous page*

Group	Average dry weight (g)	Area under the curve	Average area under the curve	Standard deviation of area under curve	pH level and consistency note
		150			
C5	6	195 200 200	200	4	pH 7.4, consistent
C6	6.2	220 195 200	205	10	pH 5, less consistent

To account for all the individual fluctuations, Table 4.3 was created. It shows that the area of all samples degraded in pH 5 PBS solution (C2, C4 and C6) had higher variability compared to those in pH 7.4 (C1, C3 and C5), as indicated by the higher standard deviations and the overall larger areas under the curves.
Furthermore, Figures 4.11, 4.12, and 4.13 demonstrate that the initial water uptake between one group of the samples in PBS solution with pH 5 varied more than that of samples in PBS solution with pH 7.4. This suggests that PBS solution with lower pH is absorbed more easily by PLA than PBS solution with higher pH. Therefore, I conclude that increased acidity leads to greater interaction between ions and PLA, resulting in higher absorption.
Another observation is that the mean dry weight of the samples does not increase by the same factor as the area under the curve for the wet weight samples. This suggests a faster degradation of the samples with less infill, due to a proportionally higher average area, which aligns with the fact that samples with less infill degrade faster.
The high standard deviations in Fig. 4.13 may be attributed to several factors, such as imprecise measurements, since the samples were simply taken out of the solutions and some might have more water attached to their surface than others. Additionally, printing defects could alter the water uptake, as seen in some samples by bulging at the top or bottom. Due to printing errors and weaknesses at the bottom of the samples, it was noticed that small particles fell off all samples after 35 days, regardless of the pH.

The degradation of PLA samples is influenced by their structure and by hydrolysis conditions such as temperature. The temperature of the dissolution bath fluctuated between 25°C and 43°C, with a tendency to remain around 28°C, rather than maintaining the desired body temperature of 37°C. This temperature is suboptimal and low for the degradation of PLA, which has a Tg of approximately 60°C [75]. The lower temperature does not facilitate faster degradation of PLA. PLA is known to degrade over a period of 1 to 5 years at a temperature of 37°C in PBS [68].
The degradation of the samples also depends on their prehistory. Since the samples were 3D printed, the high printing temperature results in degradation that produces more mobile chains, which in turn induce crystallization. The increased crystallinity

of the samples makes it more difficult for water to penetrate compared to the amorphous regions, as the structure is more rigid [75].

4.3.2 PLGA/PI degradation

For degradation testing, samples with PLGA/PI ratios of 80:20 and 90:10 w/w were selected due to their demonstrated potential (see Tab.4.2). Each basket contained three samples, measuring approximately 1.2 cm in diameter and 1-2 mm in height, although precise measurements were challenging due to their uneven structure.
Within a day, most samples fused into larger pieces (Fig. 4.16), probably due to the PI stickiness, while those remaining separate struggled to maintain shape, often curling within the baskets.

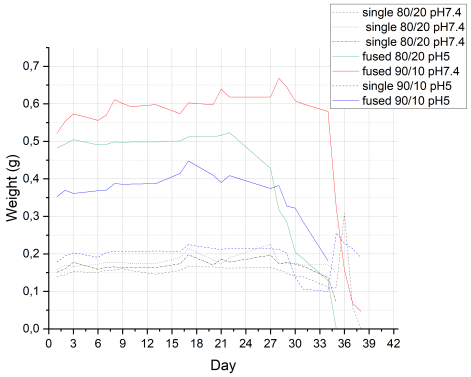

Figure 4.14: Degradation of individual PLGA/PI samples

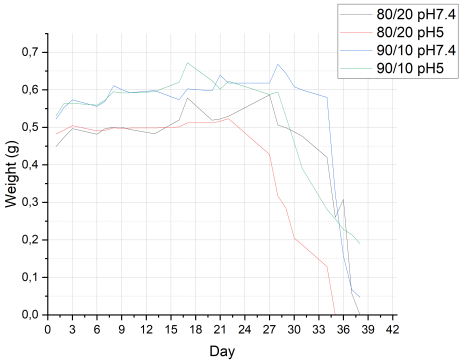

Figure 4.15: Degradation of PLGA/PI samples, grouped by composition and degradation pH

Fig. 4.14 illustrates the degradation of individual samples saved from fusion as well as larger fused pieces. Due to varying degradation speeds, some samples became unrecognizable, hindering individual weight measurement. Therefore, remaining contents in the baskets were measured after day 34, marking the end of Fig. 4.14. To present a comprehensive degradation picture, Fig. 4.15 plotted total weights of three samples of the same composition in different pH degradation environments.

The observed wrinkling phenomenon (see Fig.4.19) may result from PI and PLGA's high viscosity and hydrophobic nature, leading to rapid microsphere surface solidification [78]. Initially, bubbles appeared on the samples surface, transforming into wrinkles over three weeks (Fig.4.18). Non-uniform liquid uptake of PBS likely occurred, which was noticed in weight increase of all samples.The wrinkling of the samples could also be associated with the PLGA microparticles that exhibit lower pH at their cen-

Figure 4.16: Fusion of two samples

ters due to autocatalytic degradation product activity [76]. Additionally, PLGA and PI may re-orient as water penetrates, potentially weakening surfaces. PLGA's Tg is $\sim$ 37°C [58]; apparatus temperature fluctuations (reaching 43°C) may have induced slight structural loosening, leading to orientation.
Upon water immersion, samples hardened when they were tested by squeezing them together, possibly due to trapped water from small pore sizes.
Increasing brittleness, loss of brown color, and a paler appearance were observed throughout the experiment, as shown in Fig. 4.19. Notable differences emerged between samples exposed to pH 7.4 and pH 5 PBS. After approximately three weeks, pH 7.4 samples displayed pronounced wrinkling and brittleness, retaining their shape. In contrast, pH 5 samples appeared bloated with fewer wrinkles, indicating faster degradation, aligning with PLGA degradation rates [77]. pH 7.4 samples fused with the basket (Fig. 4.17), while pH 5 samples began melting, suggesting reduced mechanical strength and increased PBS absorption. The parts that melted out of the basket sank to the bottom, retaining a perfectly spherical and homogeneous shape. Upon removal from the water, almost immediate phase separation occurred, as illustrated in Fig. 4.18. This undesired outcome suggests that a different basket design will help to obtain more comparable and consistent results.

Table 4.4: Areas under the curves and dry weights of different groups for PLGA/PI samples

Composition (PLGA/PI w/w)	**pH of PBS solution**	**Average dry weight (g)**	**Area under the curve**
80/20	7.4	0.17	10
80/20	5	0.17	8
90/10	7.4	0.19	12
90/10	5	0.19	12

In Table 4.4, the areas under the curves in Fig.4.15 were calculated. The results indicate that the areas of the pH 7.4 samples are larger, reflecting a slower degradation rate. Additionally, the difference in areas between different pH levels is more pronounced in the 80/20 samples compared to the 90/10 samples.
It is important to note that the samples, which have a diameter of 1.2 cm and a height of 1-2 mm, are relatively small. Due to attachment and fusion issues within the baskets, the measurements are not reliable. Consequently, no definitive conclusions can be drawn about the degradation rates of the samples over time based on these measurements.

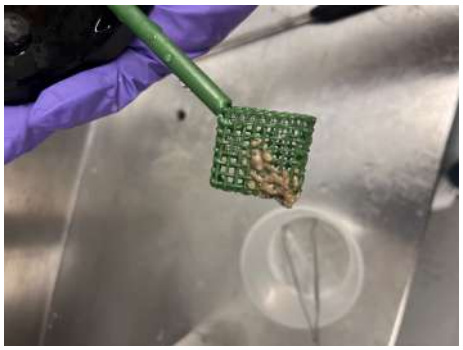

Figure 4.17: Fusion of sample with basket

From Figs. 4.14 and 4.15, it is evident that samples in PBS solution with pH 5 begin to lose weight approximately three days before those with pH 7.4. Generally, all samples start losing weight after three weeks. After one month, the samples in pH 7.4 degrade slightly slower than those in pH 5. However, after five weeks, it can be observed that the 80/20 samples in pH 7.4 degrade completely (see Fig.4.15).
The accuracy of these results is limited due to the baskets' large grids, which caused samples to get partially stuck or disintegrate and fall through the holes. Sample fragments could still be seen at the bottom of the container for the pH 7.4 samples, making visual and tactile inspections more reliable.
Additionally, the surface areas between the samples varied due to the sample fusion. The 80/20 samples in pH 7.4, which remained separate, showed a similar degradation pattern to the 90/10 samples in pH 7.4 (see Fig.4.15). These three samples fused into one large sample, reducing the surface area. It can be hypothesized that the higher PLGA content in the 90/10 samples would result in a slightly longer degradation time.
In the pH 5 samples, the 80/20 samples fused together, while in the 90/10 group, one sample remained separate, and the other two fused. These two curves exhibit similar behavior, but the 90/10 samples had a larger surface area. Therefore, no definitive conclusion can be drawn from the graphs.
It is also worth noting that the PI components of the samples cannot be fully analyzed due to the unknown properties of PI. If it is natural, it contains more proteins than synthetic PI, and if treated with ammonia to enhance colloidal stability during storage , its properties may be further altered [79].

Figure 4.18: Wrinkly samples, with droplet in the center

(a) Day 1 **(b)** Day 26 **(c)** Day 33

Figure 4.19: Samples PLGA/PI 80/20 w/w in pH 7.4 PBS solution

5

Conclusion

The aim of this thesis was to reduce the potential risks associated with surgeries, specifically by aiming to prevent the need for a second surgery in infants.
This necessity was identified after discussions with surgeons and anesthesiologists at Sahlgrenska Hospital who expressed satisfaction with the surgical technique but were dissatisfied with the requirement to remove stainless steel springs. This led to the need for the development of new materials.
Although there is a wide range of materials and structures available, I chose to focus on the PLGA/PI blend as it appeared promising based on literature. The final concept of creating a filament of PLGA/PI and 3D printing the implants revealed several challenges that I addressed in my thesis.
After analyzing PLA and exploring its 3D printing capabilities, several conclusions can be drawn. Initially, it became evident that the desired shapes could not be achieved with the available 3D printers due to size limitations. Therefore, a more precise and finer 3D printer is required.
Nevertheless, samples four times larger than the initial ones were printed with various infill patterns and percentages to assess their compression strength and degradation time. From these experiments, it was evident that pure PLA samples were too robust to replace the stainless steel springs.
Additionally, the degradation of the PLA samples proved to be excessively slow, potentially posing a problem as infant skull plates typically fuse within the first 10 months of life. Moreover, no significant differences were observed in the degradation rates of samples with different infill patterns or exposed to different pH PBS solutions.

Furthermore, selecting the right material is crucial for these implants. Despite initial success with the PLGA/PI blend, attempts to obtain mechanically testable samples were unsuccessful due to immiscibility issues and inadequate molding techniques. Consequently, it was concluded that the material can not be reproduced, owing to phase separation, even though there have been carried out successful trials and tested in rabbits.
Although the degradation of PLGA/PI samples was successful in both pH 7.4 and pH 5 solutions, indicating its potential to replace stainless steel springs, further investigation is needed to ensure that degradation occurs within the appropriate time frame. Small samples were obtained in this experiment, measuring 1.2 cm in diameter and 1-2 mm in height. However, the actual version would be U-shaped with a length of several centimeters, resulting in a larger surface area that would alter the degradation time.

Literature review and results obtained within this thesis suggest that there are yet no material solutions fulfilling the criterias to stainless steel springs used in sagittal craniosynostosis with obvious improvements as compared to current practice.

The research within this thesis involves several ethical consideration in order to protect all involved entities, with a special focus on the infants. Furthermore the research ensured potential to benefit individuals ans society as a whole. The low cost of the experiments and potential product in future would have minimal environmental effects.

Recommendations: In case of rapid degradation, consideration could be given to PLGA with a higher Mw. Moreover, improvements in blending and molding, may not improve the miscibility of PLGA and PI which is necessary to produce samples that are not phase-separated, ensuring uniform load-bearing capacity and degradation.
Given the individual nature of sagittal craniosynostosis, future endeavors may involve 3D printing customized springs tailored to individual needs and adjusting the infill according to the required force for skull plate separation.

Lastly, future considerations may include further exploration of PLA/PCL blends utilizing PLA with higher Mw.

Bibliography

[1] Yilmaz, E., Mihci, E., Nur, B., Alper, Ö. & Taçoy, Ş. Recent Advances in Craniosynostosis. *Pediatric Neurology.* **99** pp. 7-15 (2019,10), https://linkinghub.elsevier.com/retrieve/pii/S0887899418300699

[2] Derderian, C. & Seaward, J. Syndromic Craniosynostosis. *Seminars In Plastic Surgery.* **26**, 064-075 (2012,5), http://www.thieme-connect.de/DOI/DOI?10.1055/s-0032-1320064

[3] Kajdic, N., Spazzapan, P. & Velnar, T. Craniosynostosis - Recognition, clinical characteristics, and treatment. *Bosnian Journal Of Basic Medical Sciences.* (2017,6,17), https://www.bjbms.org/ojs/index.php/bjbms/article/view/2083

[4] Cranialcenter, https://cranialcenter.com/craniosynostosis/

[5] AAFP https://www.aafp.org/pubs/afp/issues/2004/0615/p2863.html

[6] Kabbani, H. & Raghuveer, T. Craniosynostosis. *American Family Physician.* **69**, 2863-2870 (2004,6,15)

[7] Borghi, A., Rodriguez Florez, N., Ruggiero, F., James, G., O'Hara, J., Ong, J., Jeelani, O., Dunaway, D. & Schievano, S. A population-specific material model for sagittal craniosynostosis to predict surgical shape outcomes. *Biomech. Model. Mechanobiol.*. **19**, 1319-1329 (2020,8)

[8] Hassanajili, S., Karami-Pour, A., Oryan, A. & Talaei-Khozani, T. Preparation and characterization of PLA/PCL/HA composite scaffolds using indirect 3D printing for bone tissue engineering. *Materials Science And Engineering: C.* **104** pp. 109960 (2019), https://www.sciencedirect.com/science/article/pii/S0928493119308756

[9] Faller, G., Dos Santos, L., Marques, D. & Collares, M. Development and testing of an absorbable spring for cranial expansion in rabbits. *Journal Of Cranio-Maxillofacial Surgery.* **43**, 1269-1276 (2015), https://www.sciencedirect.com/science/article/pii/S1010518215001717

[10] Cross, C., Khonsari, R., Larysz, D., Johnson, D., Kölby, L. & Moazen, M. Predicting and comparing three corrective techniques for sagittal craniosynostosis. *Sci. Rep.*. **11**, 21216 (2021,10)

[11] Swider, P., Delanoë, F., Jalbert, F., Boetto, S., Assemat, P., Estivalèzes, E. & Lauwers, F. Mechanical properties of fused sagittal sutures in scaphocephaly. *Clinical Biomechanics*. **86** pp. 105369 (2021), https://www.sciencedirect.com/science/article/pii/S0268003321000991

[12] Sangani, M. *Craniosynostosis*, 2012. Available at: `http://aiimsnets.org/NeurosurgeryEducation/NeurosurgicalSpecialties/Pediatric/Cranisynostosis%202012/Cranisynostosis%202012.pdf`

[13] Jung,Craniosynostosis. , https://acnr.co.uk/articles/craniosynostosis/

[14] Lee, B., Hwang, L., Doumit, G., Wooley, J., Papay, F., Luciano, M. & Recinos, V. Management options of non-syndromic sagittal craniosynostosis. *Journal Of Clinical Neuroscience*. **39** pp. 28-34 (2017), https://www.sciencedirect.com/science/article/pii/S0967586816313431

[15] Kajdic, N., Spazzapan, P. & Velnar, T. Craniosynostosis - Recognition, clinical characteristics, and treatment. *Bosn. J. Basic Med. Sci.*. **18**, 110-116 (2018,5)

[16] Governale, L. Craniosynostosis. *Pediatric Neurology*. **53**, 394-401 (2015), https://www.sciencedirect.com/science/article/pii/S0887899415003367

[17] Sgouros, S. Skull vault growth in craniosynostosis. *Child's Nervous System*. **21**, 861-870 (2005,3), http://dx.doi.org/10.1007/s00381-004-1112-2

[18] Berry-Candelario, J., Ridgway, E., Grondin, R., Rogers, G. & Proctor, M. Endoscope-assisted strip craniectomy and postoperative helmet therapy for treatment of craniosynostosis. *Neurosurgical Focus*. **31**, E5 (2011,8), https://thejns.org/view/journals/neurosurg-focus/31/2/2011.6.focus1198.xml

[19] Satanin, L., Teterin, I., Evteev, A., Sakharov, A., Kölby, L., Lemeneva, N. & Roginsky, V. Introduction of spring-assisted cranioplasty for scaphocephaly in Russia: first cases evaluated using detailed craniometry and principal component analysis. *Journal Of Plastic Surgery And Hand Surgery*. **53**, 173-179 (2019,2), http://dx.doi.org/10.1080/2000656X.2019.1571501

[20] Chong, S., Wang, K., Phi, J., Lee, J. & Kim, S. Minimally invasive suturectomy and postoperative helmet therapy : Advantages and limitations. *J. Korean Neurosurg. Soc.*. **59**, 227-232 (2016,5)

[21] Sindy, E., Aloudah, E., Alamani, S., Alqahtani, A., Alawad, H., Alteraigi, A., Alrawsaa, F., Alharbi, M., Sangoura, S., Shehatah, A. & Hakami, R. Evaluation, treatment, complications, and prognosis of craniosynostosis. *International Journal Of Community Medicine And Public Health*. **10**, 5055-5060 (2023,11), http://dx.doi.org/10.18203/2394-6040.ijcmph20233811

[22] Rodriguez-Florez, N., Ibrahim, A., Hutchinson, J., Borghi, A., James, G., Arthurs, O., Ferretti, P., Dunaway, D., Schievano, S. & Jeelani, N. Cranial bone structure in children with sagittal craniosynostosis: Relationship with surgical outcomes. *Journal Of Plastic, Reconstructive amp; Aesthetic Surgery*. **70**, 1589-1597 (2017,11), http://dx.doi.org/10.1016/j.bjps.2017.06.017

[23] Rodgers, W., Glass, G., Schievano, S., Borghi, A., Rodriguez-Florez, N., Tahim, A., Angullia, F., Breakey, W., Knoops, P., Tenhagen, M., O'Hara, J., Ponniah, A., James, G., Dunaway, D. & Jeelani, N. Spring-Assisted Cranioplasty for the Correction of Nonsyndromic Scaphocephaly: A Quantitative Analysis of 100 Consecutive Cases. *Plastic amp; Reconstructive Surgery.* **140**, 125-134 (2017,7), http://dx.doi.org/10.1097/PRS.0000000000003465

[24] Fischer, S., Unander-Scharin, J., Bhatti-Söfteland, M., Nysjö, J., Maltese, G., Lif, H., Tarnow, P., Enblad, P., Kölby, L. & Nowinski, D. Springs Produce Favorable Morphological Outcomes Relative to H-craniectomy According to a Two-center Comparison of Matched Cases. *Plastic amp; Reconstructive Surgery.* **Publish Ahead of Print** (2023,5), http://dx.doi.org/10.1097/PRS.0000000000010761

[25] Borghi, A., Schievano, S., Rodriguez Florez, N., McNicholas, R., Rodgers, W., Ponniah, A., James, G., Hayward, R., Dunaway, D. & Jeelani, N. Assessment of spring cranioplasty biomechanics in sagittal craniosynostosis patients. *J. Neurosurg. Pediatr.*. **20**, 400-409 (2017,11)

[26] Du, W., Bhojwani, A. & Hu, J. FACEts of mechanical regulation in the morphogenesis of craniofacial structures. *Int. J. Oral Sci.*. **13**, 4 (2021,2)

[27] Xu, D., Xu, Z., Cheng, L., Gao, X., Sun, J. & Chen, L. Improvement of the mechanical properties and osteogenic activity of 3D-printed polylactic acid porous scaffolds by nano-hydroxyapatite and nano-magnesium oxide. *Heliyon.* **8**, e09748 (2022,6)

[28] Kyutoku, S. & Inagaki, T. Review of past reports and current concepts of surgical management for craniosynostosis. *Neurol. Med. Chir. (Tokyo).* **57**, 217-224 (2017)

[29] Betances, E., Mendez, M. & Das, J. Craniosynostosis. (StatPearls Publishing,2023,8)

[30] Kleij, L., De Vis, J., Bresser, J., Hendrikse, J. & Siero, J. Arterial CO2 pressure changes during hypercapnia are associated with changes in brain parenchymal volume. *Eur. Radiol. Exp.*. **4**, 17 (2020,3)

[31] Bristol, R., Lekovic, G. & Rekate, H. The effects of craniosynostosis on the brain with respect to intracranial pressure. *Seminars In Pediatric Neurology.* **11**, 262-267 (2004,12), http://dx.doi.org/10.1016/j.spen.2004.11.001

[32] Jones, S. & Samanta, D. Macrocephaly. (StatPearls Publishing,2023,7)

[33] Coats, B. & Margulies, S. Material properties of human infant skull and suture at high rates. *J. Neurotrauma.* **23**, 1222-1232 (2006,8)

[34] Dornelles, R., Cardim, V. & Alonso, N. Skull expansion by spring-mediated bone regeneration. *Bone Regeneration.* (2012,4)

[35] Jeelani, N., Borghi, A., Florez, N., Bozkurt, S., Dunaway, D. & Schievano, S. "the science behind the Springs"-using biomechanics and finite element modeling to predict outcomes in spring-assisted sagittal synostosis surgery. *J. Craniofac. Surg.*. **31**, 2074-2078 (2020,8)

[36] Makadia, H. & Siegel, S. Poly lactic-co-glycolic acid (PLGA) as biodegradable controlled drug delivery carrier. *Polymers (Basel)*. **3**, 1377-1397 (2011,9)

[37] Elmowafy, E., Tiboni, M. & Soliman, M. Biocompatibility, biodegradation and biomedical applications of poly(lactic acid)/poly(lactic-co-glycolic acid) micro and nanoparticles. *J. Pharm. Investig.*. **49**, 347-380 (2019,7)

[38] van Veelen-Vincent, Marie Lise Charlotte. *Thesis Title*, Year. Available at: `https://pure.eur.nl/ws/portalfiles/portal/46434944/170609_Veelen-Marie-LC-van.pdf`

[39] Rachwalski, M., Khonsari, R. & Paternoster, G. Current approaches in the development of molecular and pharmacological therapies in craniosynostosis utilizing animal models. *Mol. Syndromol.*. **10**, 115-123 (2019,2)

[40] Seattle Children's. *Craniosynostosis Research and Clinical Trials*. Available at: `https://www.seattlechildrens.org/clinics/craniofacial/research-and-clinical-trials/craniosynostosis/`

[41] Oppenheimer, A., Rhee, S., Goldstein, S. & Buchman, S. Force-induced craniosynostosis in the murine sagittal suture. *Plast. Reconstr. Surg.*. **124**, 1840-1848 (2009,12)

[42] Heller, J. Uncovering the role of stress in craniosynososostosis. (Yale University,2006)

[43] Stanton, E., Urata, M., Chen, J. & Chai, Y. The clinical manifestations, molecular mechanisms and treatment of craniosynostosis. *Dis. Model. Mech.*. **15** (2022,4)

[44] Veith, A., Conway, D., Mei, L., Eskin, S., McIntire, L. & Baker, A. Effects of mechanical forces on cells and tissues. *Biomaterials Science*. pp. 717-733 (2020)

[45] Yu, M., Ma, L., Yuan, Y., Ye, X., Montagne, A., He, J., Ho, T., Wu, Y., Zhao, Z., Sta Maria, N., Jacobs, R., Urata, M., Wang, H., Zlokovic, B., Chen, J. & Chai, Y. Cranial suture regeneration mitigates skull and neurocognitive defects in craniosynostosis. *Cell*. **184**, 243-256.e18 (2021,1)

[46] Bariana, M., Kaidonis, J., Losic, D., Ranjitkar, S. & Anderson, P. Titania nanotube-based protein delivery system to inhibit cranial bone regeneration in Crouzon model of craniosynostosis. *Int. J. Nanomedicine*. **14** pp. 6313-6324 (2019,8)

[47] Yasukawa, T., Ogura, Y., Sakurai, E., Tabata, Y. & Kimura, H. Intraocular sustained drug delivery using implantable polymeric devices. *Adv. Drug Deliv. Rev.*. **57**, 2033-2046 (2005,12)

[48] Kaewsichan, L., Riyapan, D., Prommajan, P. & Kaewsrichan, J. Effects of sintering temperatures on micro-morphology, mechanical properties, and bioactivity of bone scaffolds containing calcium silicate. *Sci Asia.* **37** (2011,9)

[49] Yilmaz, B., Pazarceviren, A., Tezcaner, A. & Evis, Z. Historical development of simulated body fluids used in biomedical applications: A review. *Microchem. J.*. **155**, 104713 (2020,6)

[50] Jamuna-Thevi, K., Suleiman, M. & Sabri, S. The in vitro degradation of PLGA/nanoapatite/lauric acid composite membrane: A comparative study in phosphate buffer saline and simulated body fluid. *Macromol. Symp.*. **371**, 101-106 (2017,2)

[51] Hooper, K., Macon, N. & Kohn, J. Comparative histological evaluation of new tyrosine-derived polymers and poly (L-lactic acid) as a function of polymer degradation. *J. Biomed. Mater. Res.*. **41**, 443-454 (1998,9)

[52] Marques, D., Santos, L., Schopf, L. & Fraga, J. Analysis of Poly(Lactic-co-Glycolic Acid)/Poly(Isoprene) Polymeric Blend for Application as Biomaterial. *Polímeros Ciência E Tecnologia.* **23**, 579-584 (2013), http://dx.doi.org/10.4322/polimeros.2013.099

[53] Sim, P., Strudwick, X., Song, Y., Cowin, A. & Garg, S. Influence of Acidic pH on Wound Healing In Vivo: A Novel Perspective for Wound Treatment. *International Journal Of Molecular Sciences.* **23**, 13655 (2022,11), http://dx.doi.org/10.3390/ijms232113655

[54] Guerra, N., Cassel, J., Muniz, N., Henckes, N., Oliveira, F., Cirne-Lima, E. & Santos, L. Dense and Fibrous Membranes of Poly(lactic-co-glycolic acid)/Epoxidized Poly(isoprene): Chemical and Biological Evaluation. *Fibers And Polymers.* **22**, 2079-2089 (2021,4), http://dx.doi.org/10.1007/s12221-021-0971-4

[55] halcyon, https://www.halcyonagri.com/en/natural-rubber-structure-and-function/

[56] Guerra, N., Cassel, J., Henckes, N., Oliveira, F., Cirne-Lima, E. & Santos, L. Chemical and in vitro characterization of epoxidized natural rubber blends for biomedical applications. *Journal Of Polymer Research.* **25** (2018,7), http://dx.doi.org/10.1007/s10965-018-1542-2

[57] Vey, E., Rodger, C., Booth, J., Claybourn, M., Miller, A. & Saiani, A. Degradation kinetics of poly(lactic-co-glycolic) acid block copolymer cast films in phosphate buffer solution as revealed by infrared and Raman spectroscopies. *Polymer Degradation And Stability.* **96**, 1882-1889 (2011,10), http://dx.doi.org/10.1016/j.polymdegradstab.2011.07.011

[58] Gentile, P., Chiono, V., Carmagnola, I. & Hatton, P. An Overview of Poly(lactic-co-glycolic) Acid (PLGA)-Based Biomaterials for Bone Tissue Engineering. *International Journal Of Molecular Sciences.* **15**, 3640-3659 (2014,2), http://dx.doi.org/10.3390/ijms15033640

[59] Huang, J. & Ali, S. PLGA - A versatile copolymer for design and development of nanoparticles for drug delivery. *J Anal Pharm Res*. **12**, 72-78 (2023)

[60] sciencedirect, https://www.sciencedirect.com/topics/engineering/molecular-weight

[61] Rocha, C., Gonçalves, V., Silva, M., Bañobre-López, M. & Gallo, J. PLGA-Based Composites for Various Biomedical Applications. *International Journal Of Molecular Sciences*. **23**, 2034 (2022,2), http://dx.doi.org/10.3390/ijms23042034

[62] Balabanian, C., Coutinho-Netto, J., Lamano-Carvalho, T., Lacerda, S. & Brentegani, L. Biocompatibility of natural latex implanted into dental alveolus of rats. *Journal Of Oral Science*. **48**, 201-205 (2006), http://dx.doi.org/10.2334/josnusd.48.201

[63] Avgoustakis, K. Polylactic-co-Glycolic Acid (PLGA). *Encyclopedia Of Biomedical Polymers And Polymeric Biomaterials*. pp. 6491-6500 (2016,1), http://dx.doi.org/10.1081/e-ebpp-120013950

[64] Liengprayoon, S., Chaiyut, J., Sriroth, K., Bonfils, F., Sainte-Beuve, J., Dubreucq, E. & Vaysse, L. Lipid compositions of latex and sheet rubber from Hevea brasiliensis depend on clonal origin. *European Journal Of Lipid Science And Technology*. **115**, 1021-1031 (2013,6), http://dx.doi.org/10.1002/ejlt.201300023

[65] Khan, I., Mansha, M. & Mazumder, M. Polymer Blends. *Polymers And Polymeric Composites: A Reference Series*. pp. 1-38 (2018)

[66] Ansary, R., Awang, M. & Rahman, M. Biodegradable poly(D,L-lactic-co-glycolic acid)-based micro/nanoparticles for sustained release of protein drugs - A review. *Trop. J. Pharm. Res.*. **13**, 1179 (2014,9)

[67] Wibawa, G., Hatano, R., Sato, Y., Takishima, S. & Masuoka, H. Solubilities of 11 polar organic solvents in four polymers using the PiezoelectricQuartz sorption method. *J. Chem. Eng. Data*. **47**, 1022-1029 (2002,7)

[68] Woo, S. & Wee, J. Characterization of accelerated hydrolysis degradation of poly (lactic acid) in phosphate buffered saline solution. *Polym. Degrad. Stab.*. **223**, 110726 (2024,5)

[69] Feng, P., Jia, J., Liu, M., Peng, S., Zhao, Z. & Shuai, C. Degradation mechanisms and acceleration strategies of poly (lactic acid) scaffold for bone regeneration. *Mater. Des.*. **210**, 110066 (2021,11)

[70] Ebrahimi, F. & Ramezani Dana, H. Poly lactic acid (PLA) polymers: from properties to biomedical applications. *Int. J. Polym. Mater.*. **71**, 1117-1130 (2022,10)

[71] DeStefano, V., Khan, S. & Tabada, A. Applications of PLA in modern medicine. *Eng Regen*. **1** pp. 76-87 (2020,9)

[72] Rochette, A., Malenfant Rancourt, M., Sola, C., Prodhomme, O., Saguintaah, M., Schaub, R., Molinari, N., Capdevila, X. & Dadure, C. Cerebrospinal fluid volume in neonates undergoing spinal anaesthesia: a descriptive magnetic resonance imaging study. *British Journal Of Anaesthesia*. **117**, 214-219 (2016,8), http://dx.doi.org/10.1093/bja/aew185

[73] Lauritzen, C. & Tarnow, P. Craniofacial surgery over 30 years in Göteborg. *Scand. J. Surg.*. **92**, 274-280 (2003)

[74] Velghe, I., Buffel, B., Vandeginste, V., Thielemans, W. & Desplentere, F. Review on the Degradation of Poly(lactic acid) during Melt Processing. *Polymers (Basel)*. **15** (2023,4)

[75] Gorrasi, G. & Pantani, R. Hydrolysis and biodegradation of poly(lactic acid). *Synthesis, Structure And Properties Of Poly(lactic Acid)*. pp. 119-151 (2017)

[76] Ducheyne, P., Healy, K., Hutmacher, D., Grainger, D. & James Kirkpatrick, C. Comprehensive biomaterials. (Elsevier Science,2011,10)

[77] Wu, X. & Wang, N. Synthesis, characterization, biodegradation, and drug delivery application of biodegradable lactic/glycolic acid polymers. Part II: Biodegradation. *J. Biomater. Sci. Polym. Ed.*. **12**, 21-34 (2001,1)

[78] Zhang, H., Yang, Z., Wu, D., Hao, B., Liu, Y., Wang, X., Pu, W., Yi, Y., Shang, R. & Wang, S. The effect of polymer blends on the in vitro release/degradation and pharmacokinetics of moxidectin-loaded PLGA microspheres. *Int. J. Mol. Sci.*. **24** (2023,9)

[79] Payungwong, N., Sakdapipanich, J., Wu, J. & Ho, C. The interplay of protein hydrolysis and ammonia in the stability of Hevea rubber latex during storage. *Polymers (Basel)*. **15** (2023,12)

DEPARTMENT OF SOME SUBJECT OR TECHNOLOGY
CHALMERS UNIVERSITY OF TECHNOLOGY
Gothenburg, Sweden
www.chalmers.se

CHALMERS
UNIVERSITY OF TECHNOLOGY